



**HAL**  
open science

## Formation of Secondary Nitroaromatic Compounds in Polluted Urban Environments

D. Cai, X. Wang, C. George, T. Cheng, H. Herrmann, X. Li, J. Chen

► **To cite this version:**

D. Cai, X. Wang, C. George, T. Cheng, H. Herrmann, et al.. Formation of Secondary Nitroaromatic Compounds in Polluted Urban Environments. *Journal of Geophysical Research: Atmospheres*, 2022, 127 (10), pp.e2021JD036167. 10.1029/2021JD036167. hal-03689851

**HAL Id: hal-03689851**








**<https://hal.science/hal-03689851>**

Submitted on 12 Oct 2023

**HAL** is a multi-disciplinary open access archive for the deposit and dissemination of scientific research documents, whether they are published or not. The documents may come from teaching and research institutions in France or abroad, or from public or private research centers.

L'archive ouverte pluridisciplinaire **HAL**, est destinée au dépôt et à la diffusion de documents scientifiques de niveau recherche, publiés ou non, émanant des établissements d'enseignement et de recherche français ou étrangers, des laboratoires publics ou privés.

## Formation of Secondary Nitroaromatic Compounds in Polluted Urban Environments

Dongmei Cai<sup>1</sup> , Xinke Wang<sup>2</sup> , Christian George<sup>2</sup> , Tiantao Cheng<sup>3</sup> , Hartmut Herrmann<sup>4</sup> , Xiang Li<sup>1</sup> , and Jianmin Chen<sup>1</sup> 

<sup>1</sup>Shanghai Key Laboratory of Atmospheric Particle Pollution and Prevention (LAP<sup>3</sup>), Department of Environmental Science and Engineering, Fudan University, Shanghai, China, <sup>2</sup>CNRS, IRCELYON, University Lyon, Université Claude Bernard Lyon 1, Villeurbanne, France, <sup>3</sup>Department of Atmospheric and Oceanic Sciences, Institute of Atmospheric Sciences, Fudan University, Shanghai, China, <sup>4</sup>Leibniz-Institut für Troposphärenforschung (IfT), Leipzig, Germany

### Special Section:

Atmospheric PM<sub>2.5</sub> in China: physics, chemistry, measurements, and modeling

### Key Points:

- The total number and abundance of detected Nitroaromatic compounds (NACs) increased significantly during air pollution episodes
- The quantified NACs exhibited higher levels in winter than summer, largely owing to air masses passing through northern heating regions
- Controlling NO<sub>x</sub> and aromatic volatile organic compounds emissions could significantly reduce the NAC formation

### Supporting Information:

Supporting Information may be found in the online version of this article.

### Correspondence to:

X. Li and J. Chen,  
lixiang@fudan.edu.cn;  
jmchen@fudan.edu.cn

### Citation:

Cai, D., Wang, X., George, C., Cheng, T., Herrmann, H., Li, X., & Chen, J. (2022). Formation of secondary nitroaromatic compounds in polluted urban environments. *Journal of Geophysical Research: Atmospheres*, 127, e2021JD036167. <https://doi.org/10.1029/2021JD036167>

Received 8 NOV 2021  
Accepted 26 APR 2022

### Author Contributions:

**Conceptualization:** Xiang Li  
**Project Administration:** Hartmut Herrmann  
**Software:** Xinke Wang  
**Supervision:** Tiantao Cheng  
**Writing – original draft:** Dongmei Cai  
**Writing – review & editing:** Christian George, Jianmin Chen

**Abstract** Nitroaromatic compounds (NACs) are important light absorption contributors to atmospheric brown carbon; however, their formation pathways and the key influential factors in polluted urban atmospheres are largely unknown. Herein, we present the molecular characterization of atmospheric particulate NACs in urban Shanghai by applying ultra-high-performance liquid chromatography coupled to Orbitrap mass spectrometry, and investigated their seasonal and diel variations and formation pathways. The total number and abundance of NACs increased significantly during air pollution episodes, and these NACs exhibited the greatest relative abundance among CHON compounds. The 12 quantified NACs exhibited higher levels in winter ( $52.3 \pm 29.1 \text{ ng m}^{-3}$ ) than summer ( $7.83 \pm 3.30 \text{ ng m}^{-3}$ ), largely owing to air masses mostly passing through northern heating regions. Among NACs, 4-nitrophenol and 4-nitrocatechol were the most abundant species. Most of NACs were enhanced via photooxidation during the day in summer, while the day-night variations in winter were not as obvious. Further analysis of atmospheric formation relevance suggested that nitrophenol and its methylated derivatives were mainly formed through gas-phase photochemical reactions, whereas aqueous-phase oxidation processing could be an important pathway to form methyl-nitrocatechols. Formation of NACs was relatively sensitive to NO<sub>2</sub> under low-NO<sub>x</sub> conditions, and became independent of NO<sub>2</sub> under high-NO<sub>x</sub> conditions. A larger fraction of NO<sub>2</sub> was transformed into NACs than into inorganic nitrate products when nitrate was less abundant, implying that NACs would play more important roles in aerosol properties with the decline in nitrate concentrations.

## 1. Introduction

Atmospheric nitroaromatic compounds (NACs) are a class of aromatic species with both hydroxyl (–OH) and nitro groups (–NO<sub>2</sub>) connecting to a benzene ring. They not only are important atmospheric pollutants that have proved to be genotoxic and phytotoxic (Fernandez et al., 1992; Grundlingh et al., 2011; Q. G. Huang et al., 1995; Purohit & Basu, 2000), but also can affect climate and air quality (Laskin et al., 2015; Moise et al., 2015). Moreover, NACs, including nitrophenols and their derivatives (NPs), nitrocatechols and their derivatives (NCs), nitrosalicylic acids (NSAs), and nitroguaiacols (NGs), have been proven to be potentially important light absorption contributors to atmospheric brown carbon (BrC) (X. R. Li et al., 2020; Mohr et al., 2013; Teich et al., 2017; Xie et al., 2017, 2019), up to 50%–80% of the total visible light absorption (>400 nm) by BrC emitted from biomass burning (Lin et al., 2017). Therefore, elucidating the formation mechanisms and pollution characteristics of atmospheric NACs has become a major atmospheric research topic in recent years.

NACs have been observed in various ambient atmospheres, including mountain (L. Wang et al., 2018), rural (Liang et al., 2020; Mohr et al., 2013; Teich et al., 2017), suburban (Kitanovsli, Shahpoury, et al., 2020), and urban (Ikemori et al., 2019; M. Li et al., 2020; X. Li et al., 2020) environments. Combustion of biomass and fossil fuel are predominant primary sources of particulate NACs (Kitanovski et al., 2012; Mohr et al., 2013). A recent study has reported that NACs related to fresh or aged biomass burning (BB) aerosols accounted for 10%–21% of the total NACs in aerosols (L. Wang et al., 2018). Ambient concentrations of particulate NACs could reach up to over 100 ng m<sup>−3</sup> during the heating season (X. Li et al., 2020; Liang et al., 2020).

Aside from primary sources, NACs might also be produced secondarily from the oxidation of anthropogenic volatile organic compounds (VOCs), including aromatic hydrocarbons (e.g., benzene, toluene, and xylene) and lignin pyrolysis products (e.g., phenol, m-cresol, guaiacol, catechol, and methylcatechol) (Harrison, Heal, &

Cape, 2005; Iinuma et al., 2010; Krofllic et al., 2015; Xie et al., 2017). For example, nitrophenols (NP), methyl-nitrophenols (MNP), and 4-nitrocatechol (4NC) could be formed from gas-phase photooxidation of benzene or toluene in the presence of  $\text{NO}_x$  (Lin et al., 2015; Sato et al., 2007; Xie et al., 2017). NP and 4NC could be formed by OH or  $\text{NO}_3$  radical-initiated oxidation of phenol and catechol in the presence of  $\text{NO}_2$ , respectively (Finewax et al., 2018; Harrison, Barra, et al., 2005). MNP and Methyl-nitrocatechols (MNC) might arise from  $\text{NO}_x$  photooxidation of m-cresol (Iinuma et al., 2010; Olariu et al., 2002; Xie et al., 2017). Moreover, Lauraguais et al. (2014) have revealed the formation of 4NC from the OH-initiated oxidation of guaiacol in the presence of  $\text{NO}_x$ . Nevertheless, this pathway appears to play only a minor role in 4NC formation under high- $\text{NO}_x$  conditions and NGs were formed as the major products (Lauraguais et al., 2014). NGs could also be formed via  $\text{NO}_3$ -initiated oxidation of guaiacol (Yang et al., 2016). In addition to the gas-phase oxidation, NAC formation can occur via aqueous-phase oxidation of aromatics (Frka et al., 2016; Krofllic et al., 2018; Vidovic et al., 2019, 2020). NPs could be formed by either photo-nitration of phenol upon UV irradiation of nitrite (Vione et al., 2001), or by hydroxylation and nitration of benzene in the presence of nitrite/nitrous acid ( $\text{NO}_2^-/\text{HNO}_2$ ) in aqueous solutions (Vione et al., 2004). The electrophilic substitution of 3-methylcatechol (3MC) with nitronium ion ( $\text{NO}_2^+$ ) and the direct involvement of  $\text{HNO}_2$  in the nighttime transformation of 3MC via consecutive oxidation and conjugated addition reactions have been proposed as two important aqueous-phase formation pathways of MNC (Frka et al., 2016; Vidovic et al., 2018). Figure S1 in Supporting Information S1 summarized the proposed dominant reaction pathways for secondary formation of NP, NC, MNP, MNC, and NG. Additionally, it has been proposed that the atmospheric chemical sinks of NACs in the gas and aqueous phases include reactions with OH radicals (Bejan et al., 2007),  $\text{NO}_3$  radicals (Atkinson et al., 1992; Vione et al., 2009), or chlorine atoms (Bejan et al., 2015) as well as photolysis (Bejan et al., 2007; Yuan et al., 2016). However, to date, the atmospheric relevance of these processes has not been fully elucidated.

Field observations spanning from clean to polluted conditions are imperative for better revealing previously unrecognized factors and further corroborating the mechanistic understanding achieved from smog chamber experiments. However, such studies are still scarce, especially those conducted in polluted atmospheres with high levels of both  $\text{NO}_x$  and anthropogenic VOCs, where the dynamics and abundance of atmospheric oxidants and pivotal precursors of NAC formation as well as the main sources of NACs could be significantly different from those in cleaner environments. In this study, we used ultra-high-performance liquid chromatography (UHPLC) coupled with an Orbitrap mass spectrometry (MS) to characterize the molecular composition of particulate NACs in urban Shanghai across the summer and winter of 2017, and quantify some highly abundant NACs. The aim is to get an understanding of the NAC formation and major influence factors in polluted atmospheres by comparatively examining the abundance and composition of NACs under contrasting atmospheric conditions, such as, summer versus winter, daytime versus nighttime, low versus high  $\text{NO}_x$ , and low versus high nitrate. This study provides insights into formation characteristics of NACs via primary sources and secondary gas/aqueous-phase oxidation, and assesses the potential effects of severe anthropogenic pollutants (e.g., anthropogenic VOCs,  $\text{NO}_x$ , and nitrate) on NAC formation in urban areas.

## 2. Materials and Methods

### 2.1. Aerosol Sampling and Chemical Analysis

Aerosol sampling took place at a height of 15 m on the rooftop of a building at Xuhui district, Shanghai, China ( $31^\circ 10' \text{N}$ ,  $121^\circ 25' \text{E}$ ), which is located in a typical urban area surrounded by a traffic artery, residential areas, and commercial buildings, with no significant pollution sources nearby (see map in Figure S2 of Supporting Information S1).  $\text{PM}_{2.5}$  samples were collected during summer (July 18–27 plus August 3–12, 2017) and winter (16 December 2017–2 January 2018). Sampling times were during the day (07:00–18:30) and night (19:00–06:30), resolving the diel pattern of NACs formation. In total, 72  $\text{PM}_{2.5}$  samples and 4 field blanks were acquired. The details of aerosol sampling, observations of air quality and meteorological parameters (Table S1 in Supporting Information S1) and VOCs (e.g., isoprene, methyl vinyl ketone (MVK), methacrolein (MACR), benzene, and toluene), and chemical analysis of the major  $\text{PM}_{2.5}$  components (e.g., OC, EC, Inorganic ions, and levoglucosan), as well as calculation of aerosol liquid water content (ALWC) and acidity, are described in Appendix S1 of the Supporting Information S1.

## 2.2. UHPLC-Orbitrap MS Analysis

A five-step extraction procedure was used for the sample separation (i.e., extraction by methanol containing 30  $\mu$ L of saturated EDTA solution, filtration through a polytetrafluoroethylene membrane, evaporation by  $N_2$ , reconstitution by methanol, and centrifugation). The extracts were analyzed by means of an UHPLC system (Dionex UltiMate 3,000, Thermo Electron, Inc.) coupled with a Q-Exactive Orbitrap MS (Thermo Electron, Inc.). The electrospray ionization (ESI) source was operated in negative ionization mode. The scanning range of  $m/z$  was from 90 to 600 with a mass resolution of 140 000 at  $m/z$  200. The commercially available authentic standards included 4-nitrocatechol (4NC), 4-methyl-5-nitrocatechol (4M5NC), 4-nitrophenol (4NP), 2-methyl-4-nitrophenol (2M4NP), 3-methyl-4-nitrophenol (3M4NP), 2,6-dimethyl-4-nitrophenol (2,6DM4NP), 5-nitrosalicylic acid (5NSA), 3-nitrosalicylic acid (3NSA), 3-hydroxy-5-nitrobenzoic acid (3H5NA), and 4-nitroguaiacol (4NG). 4-nitrophenol-2,3,5,6- $d_4$  was used as the internal standard (IS). The recoveries of 10 NAC standards were in the range of 91.3–105% (Table S2 in Supporting Information S1). More details regarding sample extraction, instrumental analysis, and quality control of analysis are provided in Appendix S1.2 of Supporting Information S1.

Table S3 lists the retention times and molecular structures of all quantified NAC species. The target NACs were quantified by comparing their retention time and mass spectra with authentic standards or with surrogate species with the same molecular formula. The extracted ion chromatograms of NACs from the authentic standards and an ambient sample are shown in Figure S3 of Supporting Information S1. 4M5NC was identified based on its retention time matching that of the authentic standard, while 3M5NC and 3M6NC were tentatively assigned based on their corresponding fragmentation patterns (Figure S4 in Supporting Information S1). As it has been previously documented, the MS/MS product ion spectra for methyl-nitrocatechols (MNC, namely, 4M5NC, 3M5NC, and 3M6NC) differ only in relative abundances of ions corresponding to the neutral losses of NO ( $m/z$  138) and HNO ( $m/z$  137), the loss of  $NO_2$  ( $m/z$  122), and the concurrent loss of NO and CO ( $m/z$  109) (Frka et al., 2016; Iinuma et al., 2010; Kelly et al., 2010). However, the MS/MS spectrum of the compound eluting at 16.8 min in ambient aerosol extracts showed one additional peak at  $m/z$  151 (Figures S3b and S4d in Supporting Information S1), corresponding to neutral losses of  $\bullet OH$ , which agreed well with the fragmentation pattern of 3M6NC in Frka et al.'s study (Frka et al., 2016). This difference can be ascribed to the ortho effect, that is, the nitro group in 3M6NC is adjacent to one of the hydroxyl groups. Thus, the chromatographic peak at 16.8 min in our field samples was assigned to the 3M6NC isomer (Figure S3b in Supporting Information S1). The elution order of the three MNC isomer peaks in this work was similar to previous chamber experiments (Iinuma et al., 2010; Xie et al., 2017). 3M5NC and 3M6NC were quantified based on the standard curve of 4M5NC due to the lack of authentic standards and their structural similarity to 4M5NC. For the three dimethyl-nitrophenol (DMNP) isomers, 2,6DM4NP standard was used to quantify total DMNP, whereas we cannot categorically exclude the other two DMNP isomers potentially being ethyl-nitrophenols or methoxylated isomers.

## 2.3. Data Processing

The obtained chromatogram-mass spectrometry data were processed with a MZmine-2.30 software (<http://mzmine.github.io>), to obtain the  $m/z$  ratios, formulas, retention times, and peak areas of detected organic compounds (Hu et al., 2016; X. Wang et al., 2020). The molecular formula assignment was mainly based on detected  $m/z$  values with a mass tolerance of  $\pm 2$  ppm. For chemical formula  $C_cH_hO_oN_n$ , the double bond equivalent (DBE) is calculated as  $DBE = (2c + 2 + n - h)/2$ , and the aromaticity equivalent ( $X_c$ ) is calculated as  $X_c = (3DBE - 1.5o - 2)/(DBE - 0.5o)$ .  $X_c$  has been suggested to help identification and characterization of monocyclic and polycyclic aromatic compounds, with  $X_c \geq 2.50$  and  $X_c \geq 2.71$  as unambiguous minimum criteria for the presence of monocyclic and polycyclic aromatic compounds, respectively (Yassine et al., 2014). In addition, Kendrick mass defect (KMD) is useful to differentiate groups of similar compounds among a large set of molecular formulas. In this study,  $CH_2$  was chosen as a base unit, and thus, molecules with identical KMDs differ only in the number of  $-CH_2$  groups (Hughey et al., 2001). Data processing details have been described in Appendix S1.4 of Supporting Information S1 and our previous study (Cai et al., 2020). The abundance of a compound refers to its chromatographic peak area and the abundance of detected compounds were corrected using blanks. In order to facilitate more accurate comparison, relative abundance of compounds was defined as ratios of absolute abundance of each compound to that of IS (set as 100%) in the same sample.

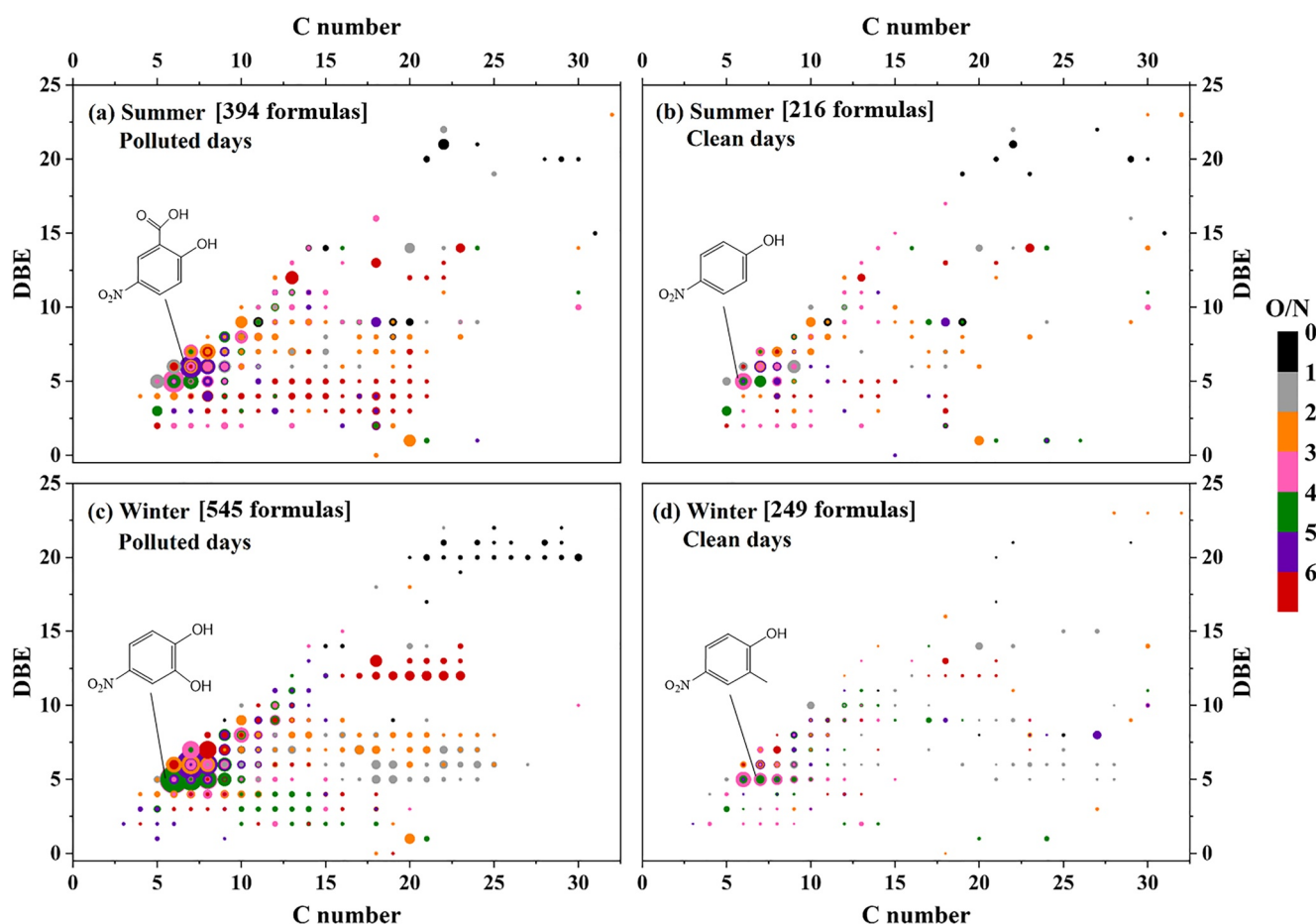


**Figure 1.** Bond equivalent (DBE) versus C number for the CHON compounds detected in polluted (a and c) and clean (b and d) days during winter and summer campaigns. The color bar denotes the oxygen-to-nitrogen ratios of CHON compounds. The marker size is proportional to the cubic root of the abundance of each compound. The formulae for the compounds with higher abundance in panels (a–d) are  $C_7H_5NO_5$ ,  $C_6H_5NO_3$ ,  $C_6H_5NO_4$ , and  $C_7H_7NO_3$ , respectively. The numbers of CHON molecular formulae in these samples are listed. Note that the proposed structures are representative and not determined.

## 2.4. Trajectory Cluster Analysis

Seventy-two-hour air mass backward trajectories arriving at the sampling location were calculated using the Hybrid Single-Particle Lagrangian Integrated Trajectory model (HYSPLIT, <http://www.arl.noaa.gov/ready/hysplit4.html>) (Rolph et al., 2017), which is conducive to investigating the transport pathways of atmospheric pollutants. The input meteorological data were obtained from the Gridded Meteorological Data Archives of the Air Resources Laboratory (<https://ready.arl.noaa.gov/archives.php>). The model was run every 4 hr, and the starting height was set at 100 m. A clustering technique, embedded in the free software TrajStat, is performed to discriminate different transport trends/tendencies in the horizontal and vertical directions (Draxier & Hess, 1998; Rolph et al., 2017). Similar trajectories are paired to form clusters in the clustering analysis, from which maximized differences are found. The cluster analysis of 72 hr backward trajectories is presented in Figure S16 of Supporting Information S1.

## 3. Results and Discussion

### 3.1. Molecular Characterization of CHON Compounds in Urban $PM_{2.5}$

By UHPLC-Orbitrap MS analysis, 216–545 measured masses were assigned to compounds containing C, H, O and N elements (CHON compounds) in ESI– mode (Figure 1). These CHON compounds were classified into 32 subgroups according to the number of N and O atoms. The total number and abundance of molecular formulae in each subgroup are shown in Figure S5 of Supporting Information S1. Based on previous studies



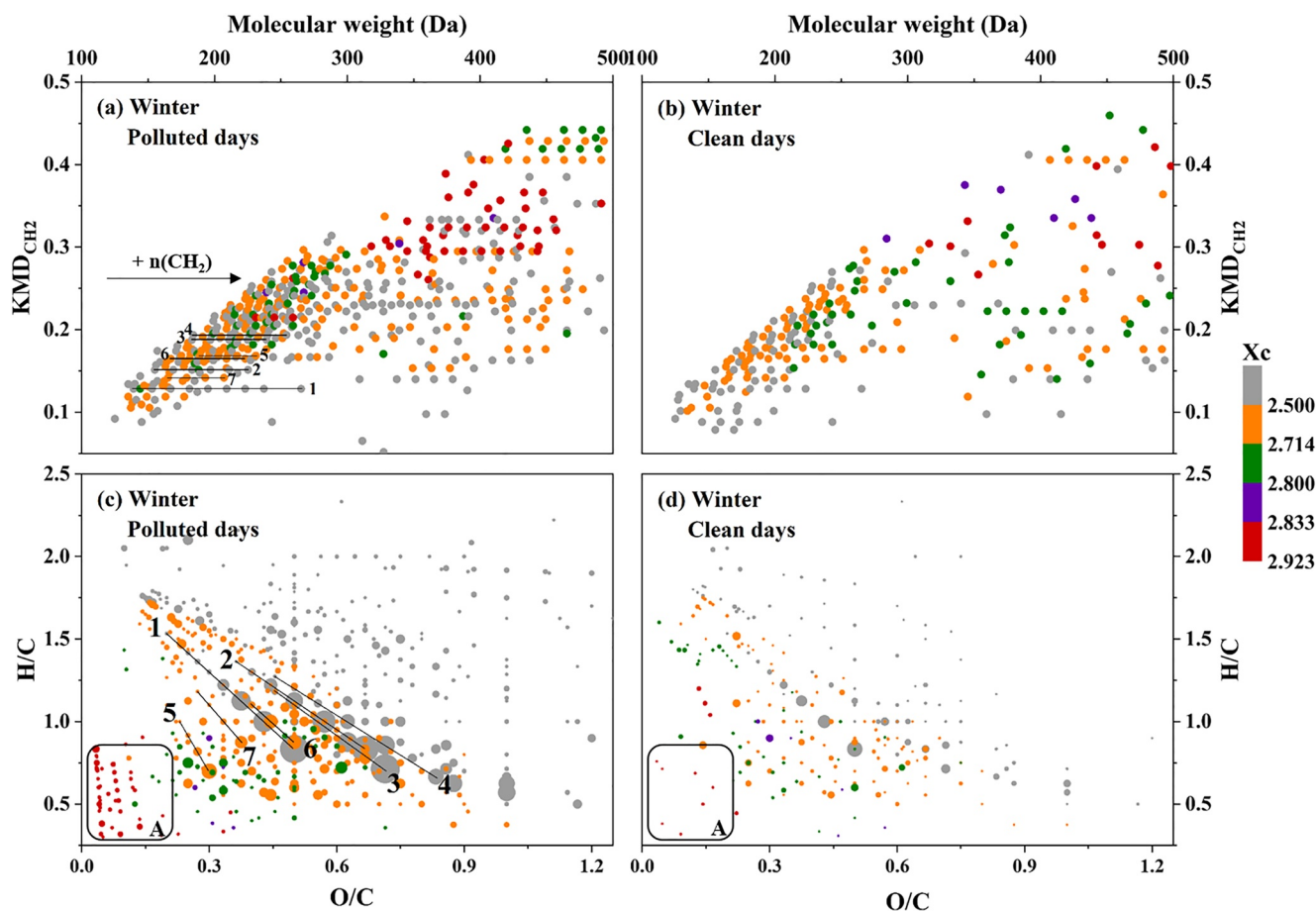
(Kourtchev et al., 2013; Laskin et al., 2009; Lin et al., 2012; Song et al., 2019), CHON compounds assigned with oxygen-to-nitrogen ratios (O/N)  $\geq 3$  could be nitro compounds or organonitrates, since these compounds appeared to contain sufficient oxygen atoms to allow the assignment of one nitro ( $-\text{NO}_2$ ) or nitrooxy ( $-\text{ONO}_2$ ) group in their formulas. Besides, the excess of O atoms in addition to those in the  $-\text{NO}_2$  functionality of CHON compounds suggests that these compounds also possess other oxygenated functional groups such as hydroxyl group ( $-\text{OH}$ ). In this study, only 53–62% of CHON compounds were characterized by O/N  $\geq 3$  (shown in the upper half of Figure S5b and S5d in Supporting Information S1), which was far lower than that in Bakersfield, USA, where this fraction was in excess of 98% (O'Brien et al., 2014). This might indicate that more CHON compounds contained reduced nitrogen functional groups (e.g., amines) in Shanghai. The majority of CHON compounds spanned a wide range of DBE values (3–25), indicating a high prevalence of double bonds and/or ring structures (Figure 1). It was obvious that almost all high-relative-abundance CHON compounds showed O/N  $\geq 3$  ( $\text{CHON}_{\text{O/N} \geq 3}$ ) and the most abundant  $\text{CHON}_{\text{O/N} \geq 3}$  species exhibited DBE 5–9, suggesting that those CHON species are mainly nitroaromatic compounds containing mono- and dinitro substituted phenols, such as nitrophenols ( $\text{C}_6\text{H}_5\text{NO}_3$ ), methyl-nitrophenol ( $\text{C}_7\text{H}_7\text{NO}_3$ ), nitrocatechols ( $\text{C}_6\text{H}_5\text{NO}_4$ ), methyl-nitrocatechols ( $\text{C}_7\text{H}_7\text{NO}_4$ ), and dinitrophenol ( $\text{C}_6\text{H}_4\text{N}_2\text{O}_5$ ), which is consistent with previous studies (Song et al., 2018, 2019; X. Wang et al., 2017). These NACs, often attributed to OA from BB in previous studies, were proposed to significantly contribute to the aerosol light absorption (Mohr et al., 2013; Teich et al., 2017; X. Zhang et al., 2013).

Figure 2 and Figure S6 in Supporting Information S1 show the  $\text{CH}_2$ -Kendrick and Van Krevelen (VK) diagrams of CHON compounds in winter and summer, respectively. Homologous compounds line up a horizontal line in the  $\text{CH}_2$ -Kendrick diagrams but a tilted one in the VK diagrams, suggesting that the homologs could have variable degrees of saturation and oxidation but possible similar structure and physicochemical properties. The CHON compounds in region A (Figures 2c and 2d and Figure S6c and S6d in Supporting Information S1) had  $X_c \geq 2.71$  and overlap with the typical region of condensed aromatic hydrocarbon (Kim et al., 2003). As it was obvious in the VK diagrams (Figures 2c and 2d and Figure S6c and S6d in Supporting Information S1), the number of CHON compounds with polycyclic aromatic characteristics in region A was significantly higher in the polluted winter samples (45 species) than during the summer (10–14 species), implying a more significant anthropogenic influence for winter samples. In addition, the number and abundance of detected NACs significantly increased in polluted days (63–85 species) compared to clean days (39–50 species), especially in winter (Figure 2 and S6 in Supporting Information S1), suggesting their potentially significant contributions to atmospheric OA during pollution episodes. It should be noted that  $X_c$  values for  $\text{C}_6\text{H}_5\text{NO}_3(\text{CH}_2)_n$  (Figures 2c-1) and  $\text{C}_6\text{H}_5\text{NO}_4(\text{CH}_2)_n$  (Figure 2c-2) are below 2.50 (e.g., aromatic compounds with  $X_c \geq 2.50$ ), implying that the number of aromatics could have been underestimated (X. Wang et al., 2017, 2020). Furthermore, the polycyclic NACs were characterized by lower H/C and O/C ratios, such as nitronaphthol homolog ( $\text{C}_{10}\text{H}_7\text{NO}_3(\text{CH}_2)_n$ , Figure 2c-5) in the lower left part of the VK diagram ( $0.5 < \text{H/C} < 1.0$  and  $0 < \text{O/C} < 0.4$ ). As mentioned above, NACs detected in this study exhibited the greatest relative abundance among CHON compounds, especially in polluted days (Figures 1 and 2 and Figure S6 in Supporting Information S1). However, the relative peak area may not accurately reflect the concentration levels of analytes, and quantification without standards is impossible because compounds with different molecular structures have different and unpredictable ionization efficiency. Because of numerous NACs detected here, using standard compounds for quantitation for all compounds was impractical, and therefore we attempted to quantify some highly abundant NACs in ambient aerosols by using 10 NAC standards in this study to further explore the compositions and formation pathways of NACs.

### 3.2. Concentration, Composition and Gas/Particle Partitioning of NACs

#### 3.2.1. Concentration and Composition of NACs

By employing authentic or surrogate standards, 12 NACs were quantified in this study and their concentrations are summarized in Figure 3 and Table S3 in Supporting Information S1. The total concentrations of NACs and their contribution to OM averaged 52.3 (12.4–118)  $\text{ng m}^{-3}$  and 0.27 (0.14–0.42) % in winter, respectively, which were about seven and five times higher than the mean concentration [7.83 (2.16–19.2)  $\text{ng m}^{-3}$ ] and contribution [0.06 (0.02–0.10) %] measured in summer. This trend agrees with previous studies in ambient aerosols from Ljubljana, Slovenia (Kitanovski et al., 2012), Hong Kong (Chow et al., 2016), Beijing (X. Li et al., 2020; Y. Wang et al., 2019), and Jinan, China (L. Wang et al., 2018). Such a seasonal variation for NACs could be associated with emission sources, formation pathways, and meteorological conditions (e.g., temperature). The clustering



**Figure 2.** (a and b)  $\text{CH}_2$ -Kendrick diagrams and (c and d) Van Krevelen diagrams for CHON compounds detected in polluted and clean days during winter. The color bar denotes the  $X_c$  values of CHON compounds. The gray, orange, green, purple, and red solid circles represent aliphatic compounds ( $X_c < 2.50$ ), aromatics with a benzene core structure ( $2.50 \leq X_c < 2.71$ ), with a naphthalene ( $2.71 \leq X_c < 2.80$ ) core structure, with an anthracene ( $2.80 \leq X_c < 2.83$ ) core structure, and with a pyrene core structure ( $2.83 \leq X_c < 2.92$ ), respectively. The marker size is proportional to the cubic root of the abundance of each compound. The molecular formulas of the homolog series 1–7 can be written as  $\text{C}_6\text{H}_5\text{NO}_3(\text{CH}_2)_n$ ,  $\text{C}_6\text{H}_5\text{NO}_4(\text{CH}_2)_n$ ,  $\text{C}_7\text{H}_5\text{NO}_5(\text{CH}_2)_n$ ,  $\text{C}_6\text{H}_4\text{N}_2\text{O}_5(\text{CH}_2)_n$ ,  $\text{C}_{10}\text{H}_7\text{NO}_3(\text{CH}_2)_n$ ,  $\text{C}_7\text{H}_5\text{NO}_4(\text{CH}_2)_n$ , and  $\text{C}_8\text{H}_7\text{NO}_3(\text{CH}_2)_n$ , respectively. Region A represents the region of highly unsaturated CHON compounds with  $X_c \geq 2.83$ , which overlapped with the typical region of condensed aromatic hydrocarbons.

analysis of backward trajectories from the sampling site (Figure S16 in Supporting Information S1) showed that the air masses in winter mainly originated from northern domestic heating regions with substantial emissions of anthropogenic pollutants (R. J. Huang et al., 2014), while the air masses mostly came from clean ocean and littoral regions in summer. As a result,  $\text{NO}_x$  that was important to electrophilic nitration of intermediates (e.g., methylcatechols) for NAC formation (Iinuma et al., 2010), exhibited an average concentration in winter about twice higher than that in summer (60.3 vs. 24.8 ppb). Meanwhile, benzene and toluene, as the precursors of NACs, also exhibited higher levels in winter ( $1.10 \pm 0.61$  ppb and  $3.07 \pm 1.52$  ppb, respectively) than summer ( $0.64 \pm 0.30$  ppb and  $1.50 \pm 0.67$  ppb, respectively) (Figure 3). Besides, BB also showed significant enhancement during winter, indicated by the four times higher level of its tracer levoglucosan in winter than in summer (251 vs. 69.4  $\text{ng m}^{-3}$  on average). Lower ambient temperatures in winter would also favor gas/particle partitioning of NACs and their intermediates. All these served to interpret the higher NACs in winter. Furthermore, based on this and previous studies, the NAC concentrations in summer are generally lowest in the four seasons (Figure S7 in Supporting Information S1), probably owing to much higher contributions from combustion emission (e.g., coal combustion and BB) in winter, spring, or autumn than in summer (Chow et al., 2016; Ikemori et al., 2019; Kahnt et al., 2013; Kitanovski et al., 2012; Kitanovski, Hovorka, et al., 2020; L. Wang et al., 2018).

The abundance of NACs also exhibited large variations in different locations (shown in Figure S7 and Table S5 of Supporting Information S1). During the summer, our measurement values ( $7.83 \pm 3.30$   $\text{ng m}^{-3}$ ) were higher

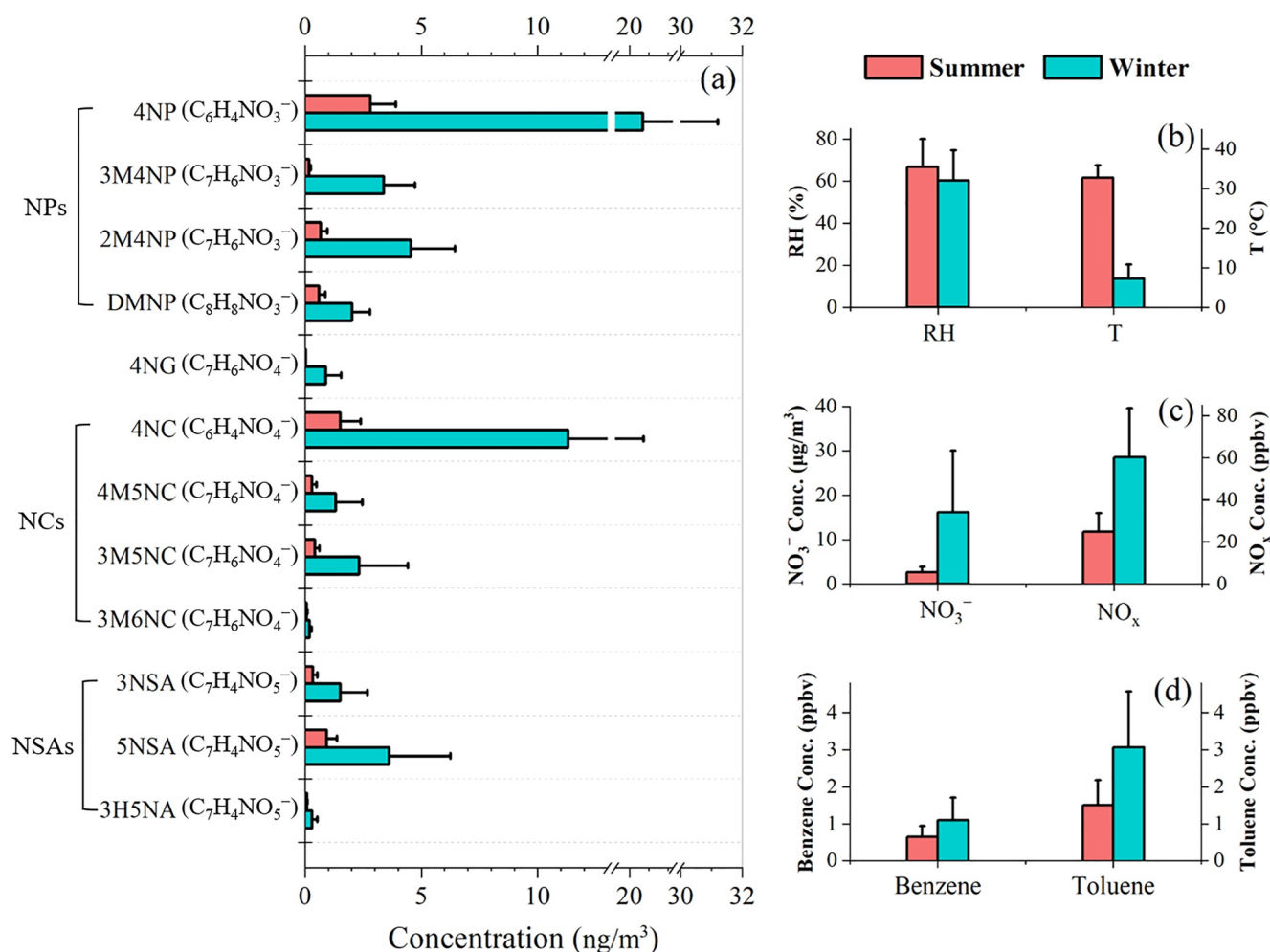


**Figure 3.** Comparison of measurements in the summer (pink) and winter (cyan) at the urban site of Shanghai, including (a) nitroaromatic compounds (NAC) concentrations, (b) RH and T, (c)  $\text{NO}_3^-$  and  $\text{NO}_x$ , and (d) anthropogenic volatile organic compounds (Benzene and Toluene). The full names, formulas, molecular weights, and molecular structures of NAC species in panel (a) are listed in Table S2 and S3 of Supporting Information S1. The error bars in panels (a–d) represent one standard variation of all data in each campaign.

than those observed in mountain, rural, and urban summer environments from China (1.87–5.9  $\text{ng m}^{-3}$ ) (Chow et al., 2016; L. Wang et al., 2018), Belgium (1.29  $\text{ng m}^{-3}$ ) (Kahnt et al., 2013), Germany (0.39  $\text{ng m}^{-3}$ ) (Teich et al., 2017), Slovenia (0.84  $\text{ng m}^{-3}$ ) (Kitanovski et al., 2012), and Japan (3.66  $\text{ng m}^{-3}$ ) (Ikemori et al., 2019), which could be attributable to the large anthropogenic emissions in Shanghai. Additionally, the total NAC level (6.51  $\text{ng m}^{-3}$ , excluding 3NSA, 3NSA, 3H5NA, and 4NG) was generally comparable to that detected in the summertime of urban Beijing (6.63  $\text{ng m}^{-3}$ ), which was under high  $\text{NO}_x$  and anthropogenic VOC conditions (Y. Wang et al., 2019). Edwards et al. (2017) showed that nocturnal oxidation of biogenic VOCs (BVOCs) would shift from low- to high- $\text{NO}_x$  regimes and that almost all of BVOCs would be oxidized by  $\text{NO}_3$  radicals at a  $\text{NO}_x/\text{BVOCs}$  ratio exceeding 1.4. As monoterpene measurements were unavailable in this study, the concentrations of BVOCs were approximated as the sum of isoprene, MVK, and MACR. The  $\text{NO}_x/\text{BVOCs}$  ratios in summer were higher than 8 (nocturnal ratios exceeding 20) (Figure S8e in Supporting Information S1). If the main anthropogenic VOCs (benzene, toluene, phenol, and cresol) are further considered,  $\text{NO}_x/\text{VOCs}$  ratios in summer were higher than 4 (nocturnal ratios exceeding 8) (Figure S8f in Supporting Information S1). A recent study reported that the  $\text{NO}_3\cdot$  oxidation in  $\text{NO}_x$ -rich air contributed significantly to the daytime NACs (Chen et al., 2021). Furthermore, the urban Shanghai in summer was under typical high- $\text{NO}_x$  conditions (Gao et al., 2019). The high- $\text{NO}_x$  environments during the campaign would promote the  $\text{NO}_3\cdot$  oxidation and  $\text{NO}_2$  nitration of aromatic alcohols (e.g., phenol and cresol) and subsequently produce abundant NACs, which explained the high levels of NACs during summer in urban Shanghai. However, the wintertime observation in Shanghai (52.3  $\text{ng m}^{-3}$ ) was much lower



than those measured in previous studies in the wintertime of Beijing ( $144.7 \text{ ng m}^{-3}$ ), Qingdao ( $121.8 \text{ ng m}^{-3}$ ), and Jinan ( $105.4 \text{ ng m}^{-3}$ ) (Figure S7 and Table S5 in Supporting Information S1), which were located in northern China and impacted by substantial emissions of anthropogenic pollutants from coal combustion and BB during the heating season (M. Li et al., 2020; X. Li et al., 2020; Liang et al., 2020). This large difference between southern and northern China further indicates that coal combustion and BB were the very important sources of NACs. Beside, compared with southern China, lower atmospheric temperatures in northern China during winter would be more favorable for the partitioning of NACs from gas phase into particle phase.

The compositions of NACs varied slightly with seasons (Figure S9 in Supporting Information S1). 4-Nitrophenol and 4-nitrocatechol were the most abundant species among all NACs quantified, accounting for 35.8% and 19.4% of the total NACs in summer and 40.0% and 21.6% of the total NACs in winter, respectively. This observation was in good agreement with recent studies, where 4NP and 4NC were the most abundant NAC species (Table S5 in Supporting Information S1) (M. Li et al., 2020; X. Li et al., 2020; Y. Wang et al., 2019). Nitrophenols and nitrocatechols could be formed from the OH radical-initiated oxidation of aromatic VOCs in the presence of  $\text{NO}_2$  (Lin et al., 2015; Vione et al., 2004; Xie et al., 2017). Moreover, 4NC has been found to predominate the composition of NAC products generated in the benzene/ $\text{NO}_x$  chamber experiment (Xie et al., 2017). Hence, it is reasonable to observe the high abundance of 4NP and 4NC in urban Shanghai under the typical high- $\text{NO}_x$  and anthropogenic VOC conditions. Notably, the contribution of 4NP could be higher if the gas-phase 4NP was considered. The concentrations of gas-phase NACs are estimated in Sect. 3.2.2 using the equilibrium absorption partitioning model. The concentrations of 4-nitroguaiacol (4NG) and its contribution to total NACs were very low, especially in summer, which coincided with recent studies (Ikemori et al., 2019; Kitanovski, Shahpoury et al., 2020). In general, the NAC compositions varied slightly with seasons in urban Shanghai and Hong Kong (Chow et al., 2016), while they in urban Jinan varied greatly with seasons (M. Li et al., 2020). This difference might be attributable to the intensified combustion of coal and biomass for domestic heating in Jinan.

### 3.2.2. Gas/Particle Partitioning of NACs

The mass transfer by gas-particle partitioning may affect the particle-phase concentrations. The gas-phase concentrations of NACs were not measured in this study. Here, the gas-phase concentrations of NACs were estimated based on their measured particle-phase concentrations and an equilibrium absorption model of gas/particle partitioning (Donahue et al., 2006; Pankow, 1994a, 1994b; Pankow et al., 2001) (see Appendix S1.5 in Supporting Information S1 for details). The saturated liquid vapor pressures of NACs were calculated using the University of Manchester multiphase system online property prediction (UManSysProp) tool (Nannoolal et al., 2008). Although vapor pressures from group contribution estimation method of Nannoolal et al. (2008) might have both structural and parametric uncertainties, Nannoolal et al. (2008) provided the comprehensive estimations of sub-cooled liquid vapor pressures of NACs.

The estimated saturation vapor pressure ( $P_L^0$ ), particle-phase fraction ( $F_p$ ), and gas-phase concentrations of NACs in summer and winter are listed in Table S4 of Supporting Information S1. The  $F_p$  of NACs varied greatly with different species and seasons. 3NSA, 5NSA, and 3H5NA ( $F_p > 99\%$ ) were almost entirely in the particle phase in both seasons. In summer, MNC (3M6NC, 3M5NC, and 4M5NC) showed substantial partitioning in the particle phase ( $F_p > 70\%$ ), while 4NP, MNP (3M4NP and 2M4NP), and DMNP were mainly in the gas phase ( $F_p < 13\%$ ). In addition, 4NG and 4NC were almost evenly distributed between the gas and particle phases. However, the  $F_p$  of NACs increased significantly from summer to winter:  $>90\%$  of MNC, 4NG, and 4NC,  $>70\%$  of DMNP, and nearly half of MNP were distributed in the particle phase, whereas only 4NP ( $F_p < 20\%$ ) was mainly in the gas phase at the relatively lower winter temperatures. This seasonal variation for the estimated  $F_p$  of NACs was consistent with a recent study on the measured  $F_p$  of NACs (Li et al., 2020b), largely attributable to the lower saturated vapor pressures of species in the lower ambient temperatures of winter. The equilibrium absorption partitioning model gives a reasonable estimation for the  $F_p$  values of NACs except for underestimation for the  $F_p$  value of 4NP and MNP (Al-Naiema & Stone, 2017; Bannan et al., 2017; M. Li et al., 2020). The estimated  $F_p$  values of 4NP and MNP in summer ( $<5\%$ ) were obviously lower than the measured  $F_p$  values in China (i.e., 15%–30% for NP and MNP in summer of 2016) (Le Breton et al., 2018; M. Li et al., 2020). Likewise, the estimated  $F_p$  values of 4NP in winter (17.7%) were generally lower than the values measured in urban Jinan, China (54% in winter), downtown Rome (82% in cold season), and Iowa City, IA USA (30% in fall) (Al-Naiema & Stone, 2017; Cecinato et al., 2005; M. Li et al., 2020). Therefore, the equilibrium absorption partitioning model might overestimate the vapor pressure of nitrophenols, which has been confirmed by Bannan et al. (2017).

Further studies for the gas-particle partitioning of NACs are warranted to better explain the potential measurement–model discrepancies and the variety of  $F_p$  values observed in different studies. Even if gas-phase NACs can also be dissolved into the aqueous phase of particles, the aerosol aqueous-phase fractions of NACs are still low given the low Henry's law constants (Sander, 2015). More details regarding the gas-particle partitioning of NACs are provided in Appendix S1.5 of Supporting Information S1.

### 3.3. Sources and Formation Pathways of NACs

Figures 4a and 4b respectively show the temporal variations of total NACs, OM, PM<sub>2.5</sub>, NO<sub>2</sub>, nitrate, K<sup>+</sup>, and benzene levels, as well as meteorological parameters during the summer and winter. Three pollution episodes were identified based on the daily mean mass concentrations of PM<sub>2.5</sub> (>75 μg m<sup>-3</sup>, Table S1 in Supporting Information S1). The concentrations of total NACs increased significantly during pollution episodes, especially in winter, which coincided with the obvious enhancements in OM, NO<sub>2</sub>, benzene, and K<sup>+</sup> (i.e., a BB tracer). During summertime, the correlation coefficient (Pearson  $r$ ) of total NACs was stronger with benzene or toluene ( $r \geq 0.69$ ) than with K<sup>+</sup> ( $r = 0.52$ ) or levoglucosan ( $r = 0.51$ ), and the total NACs correlated better with nitrate (Table S6 in Supporting Information S1,  $r = 0.52$ ,  $p < 0.01$ ) than with EC ( $r = 0.38$ ,  $p < 0.05$ ). These results indicated that NACs mainly originated from secondary formation rather than primary emissions in summer. During wintertime, the total NACs correlated strongly with levoglucosan, SO<sub>2</sub>, and CO, a widely existing byproduct from the combustion process (Table S8 in Supporting Information S1,  $r \geq 0.76$ ), suggesting more contributions of BB and coal combustion to NACs in winter. The concentrations of CO, levoglucosan, SO<sub>2</sub>, and NACs stepped up from the airflow from marine in summer to Northern China in winter (Table S1 in Supporting Information S1, Figure 3 and Figure S16 in Supporting Information S1), proclaiming that BB and coal combustion from northern outflow were important sources for NACs formation in this region. However, as levoglucosan, SO<sub>2</sub>, and CO were relatively inert and long-lifetime compounds in the atmosphere, the good correlations between them and NACs in winter could not explicitly indicate whether NACs were dominated by the direct emission or secondary oxidation of precursors emitted from BB and coal combustion sources.

A tracer method analogous to the EC-tracer method used for secondary organic carbon calculation was adopted in this study to evaluate the contributions of primary emission and secondary oxidation to the observed NACs (Chen et al., 2021; Li et al., 2019; Salvador et al., 2021; Q. Zhang et al., 2019). CO and levoglucosan were selected as the tracer for combustion and BB, respectively. The secondary formation of NACs was evaluated via Equation 1,

$$[\text{NACs}]_s = [\text{NACs}]_t - \left( \frac{[\text{NACs}]}{[\text{tracer}]} \right)_{\text{pri}} \times [\text{tracer}] \quad (1)$$

where  $[\text{NACs}]_s$  and  $[\text{NACs}]_t$  are the concentration of NACs generated from secondary oxidation and the total measured NACs, respectively,  $([\text{NACs}]/[\text{tracer}])_{\text{pri}}$  is the primary emission ratio of NACs relative to the tracer,  $[\text{tracer}]$  is the concentration of tracer.  $([\text{NACs}]/[\text{tracer}])_{\text{pri}}$  was estimated from the fitting of the minimum  $[\text{NACs}]/[\text{tracer}]$  ratio, assuming that the primary source dominated the period with minimal secondary formation.

The results from both tracers are consistent and demonstrate the dominant secondary formation of NACs during the day in winter (Table S10 in Supporting Information S1). As shown in Table S10 of Supporting Information S1, up to 59.5%–75.4% of NACs were significantly contributed by the secondary formation during the day. The fraction of secondary formation for NACs decreased at night, down to around 15.3–34.7%. Furthermore, the good correlations between O<sub>3</sub> and NACs in the daytime (Table S9a in Supporting Information S1) confirm the importance of photochemical oxidation for NACs. As reported in previous studies, the photochemical formation of NACs was related to the oxidation of aromatics in the presence of NO<sub>2</sub> (Chen et al., 2021; Finewax et al., 2018; Xu & Wang, 2013; Yuan et al., 2016). Here, the concentration of NACs increased monotonically with the increase of aromatics (Figures S12c and S13c in Supporting Information S1) in the daytime, implying the enhanced NACs formation with the increase of precursors. The apparent correlations between N<sub>2</sub>O<sub>5</sub> and NO<sub>2</sub> or NO<sub>3</sub> radical production were observed (H. Wang et al., 2018); thus, the NO<sub>2</sub> concentration was utilized as a variable to explore NO<sub>3</sub>-initiated chemistry during the sampling period. The concentration of NACs was highly correlated with NO<sub>2</sub> during the day in winter (Figure 6e and Table S9a in Supporting Information S1), indicating the significance of NO<sub>3</sub>• oxidation pathway on the daytime NACs formation. Chen et al. (2021) have shown that besides the •OH oxidation of aromatics, the NO<sub>3</sub>• oxidation also contributed significantly to the daytime NACs in NO<sub>x</sub>-rich air.

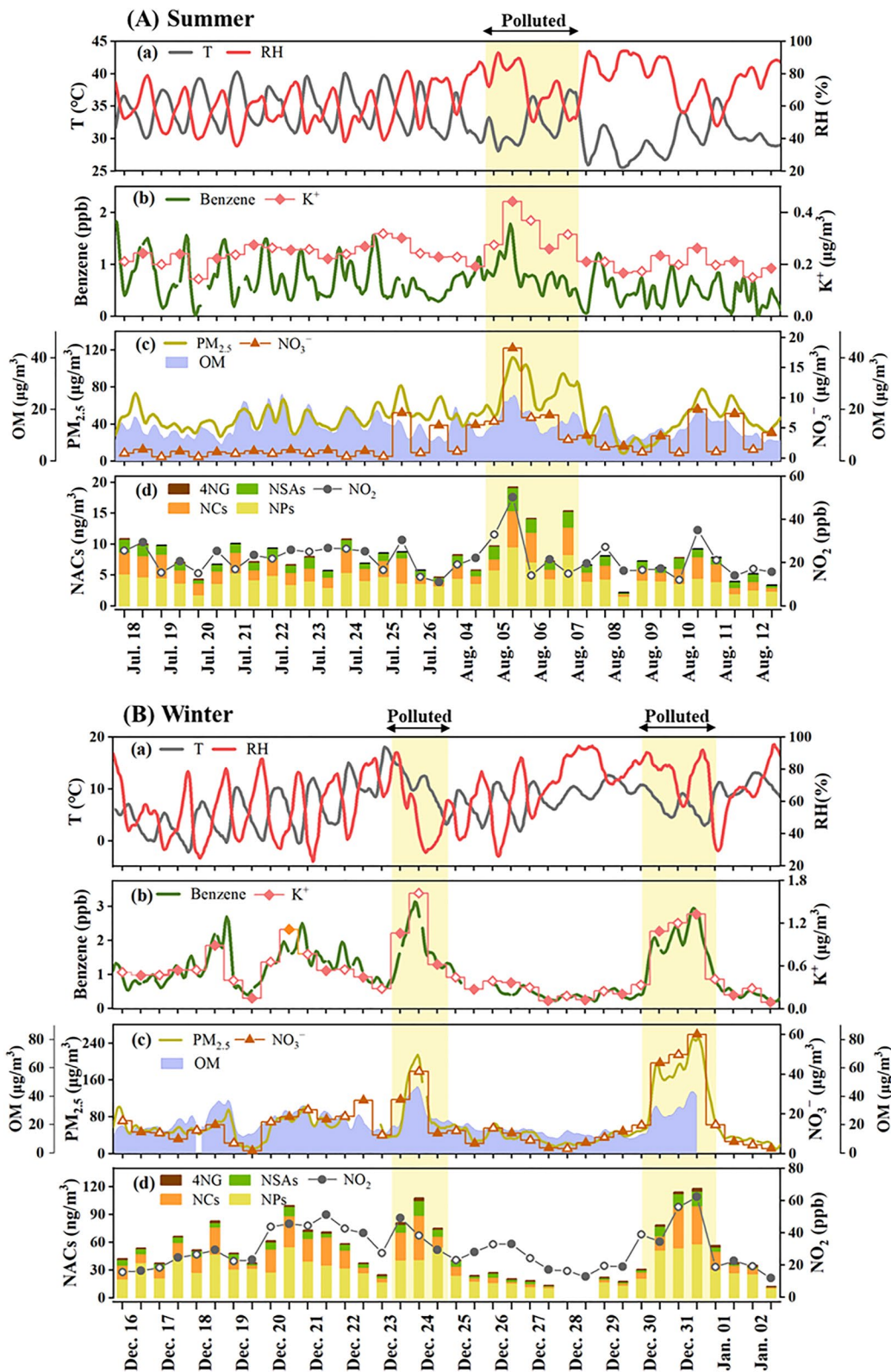


**Figure 4.** Time series of (a) temperature ( $T$ ) and relative humidity (RH), (b) benzene and  $K^+$ , (c)  $PM_{2.5}$ , OM, and nitrate, and (d)  $NO_2$  and four kinds of nitroaromatic compounds (NACs) (NPs, namely, 4NP, 3M4NP, 2M4NP, and DMNP; NCs, namely, 4NC, 4M5NC, 3M5NC, and 3M6NC; nitrosalicylic acids (NSAs), namely, 3NSA, 5NSA, and 3H5NA; 4NG) in the (a) summer and (b) winter of urban Shanghai. The empty marks denote the daytime and the solid marks denote the nighttime in panels (b–d). The pollution episodes, with elevated  $PM_{2.5}$ , are marked by light yellow shading.



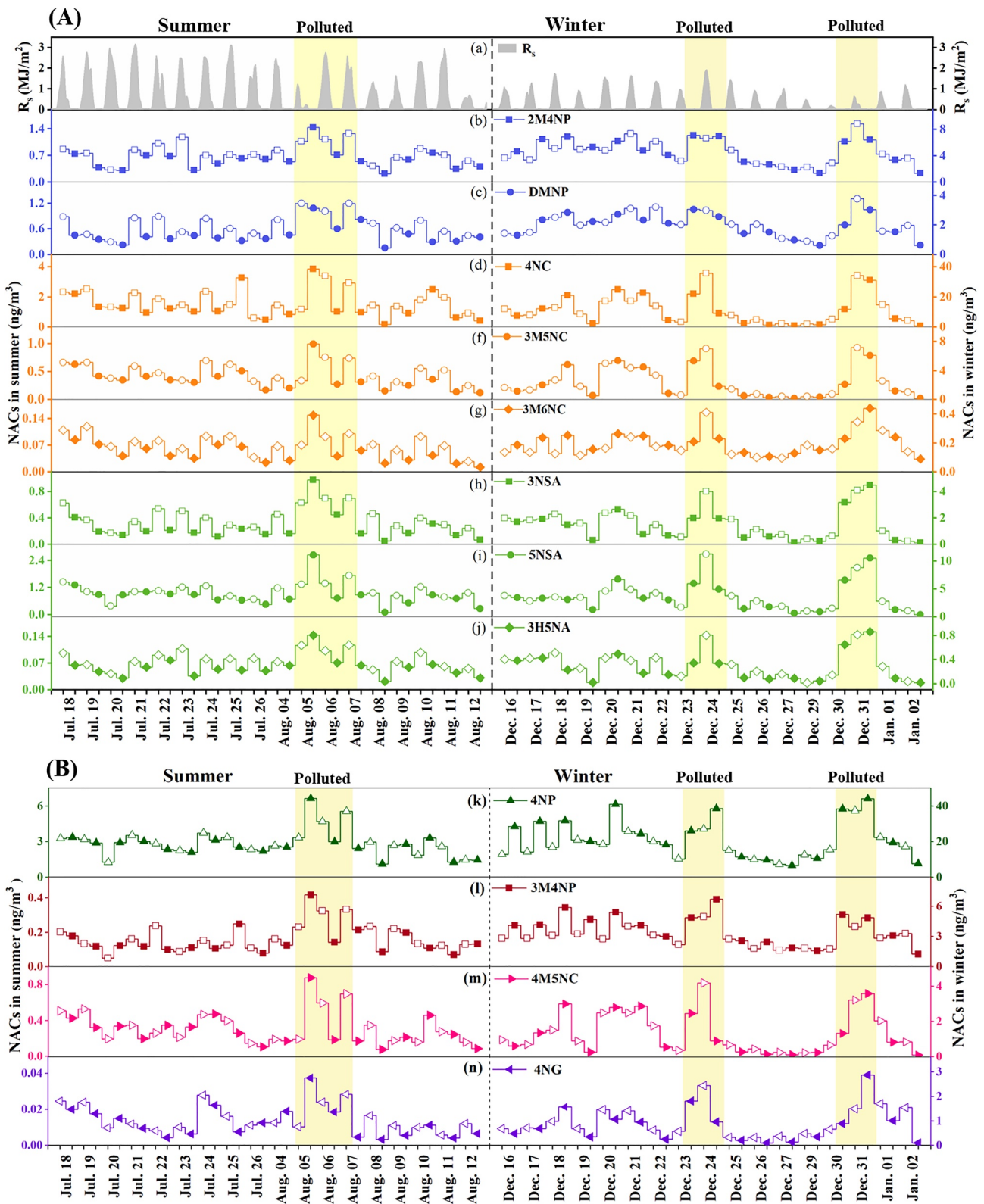


Figure 5.

To better investigate the atmospheric formation relevance, the inter-species correlations of individual NAC species and their correlations with other chemical components were examined (Tables S6 and S8 in Supporting Information S1). The inter-species correlations within each subgroup, that is, NPs ( $r \geq 0.66$ ), NCs ( $r \geq 0.79$ ), and NSAs ( $r \geq 0.82$ ), were generally stronger than those between the subgroups, for example, nitrocatechol derivatives (MNC) and nitrophenol derivatives (DMNP,  $r = 0.43\text{--}0.53$ , in summer) during the observation campaigns. This strongly suggested that the formation and loss pathways as well as their influential factors might be more similar within each subgroup than between the subgroups. Additionally, in comparison with NPs, NCs and NSAs in summer correlated better with benzene, toluene, and  $K^+$ , whereas their correlations showed no discernible difference in winter (Tables S7 and S9 in Supporting Information S1). This was possibly associated with the fact that particle-phase NPs only contribute to a minor fraction of their atmospheric abundance because of their high saturation vapor pressures in summer, especially for nitrophenols (Table S4 in Supporting Information S1). The concentration of particulate NP could largely depend on gas-to-particle partitioning, which is strongly susceptible to temperature, as well as their gas-phase loss pathways (e.g., photolysis) (Bejan et al., 2007; M. Li et al., 2020; Yuan et al., 2016). Additionally, since the majority of NCs and almost all of NSAs were distributed in the particle phase, especially in winter (Table S4 in Supporting Information S1), the photolysis and oxidation degradation rates of NCs and NSAs could be much lower. Slade and Knopf (2014) reported that, compared with the dry condition, the reactive uptake of OH by MNC aerosol particles was reduced by a factor of 4 at RH approaching 15%–30%, as a result of competitive coadsorption of  $H_2O$  that occupied reactive sites. The higher ambient RH condition (44%–92%) in this work likely further suppressed OH uptake by MNC particles, and thereby the multiphase oxidation degradation of MNC by OH was probably unimportant. Interestingly, NPs, NCs, and NSAs correlated better with levoglucosan or  $K^+$  in winter than in summer, further hinting at a greater contribution of direct BB emissions to NACs in winter than in summer. Besides, the higher ratios of NPs versus NSAs in winter than in summer (Figure S10 in Supporting Information S1) indicated that NSAs are more likely formed from oxidation of aromatic VOCs rather than direct emissions. This also explains higher proportions of NSAs in summer than in winter (17% vs. 11%, Figure S9 in Supporting Information S1).

To further elucidate the distinctive secondary formation chemistry of NACs, we examined the diel variations of individual NAC species (Figure 5). Most NAC species in summer exhibited daytime enhancements, while NAC species in winter had no obvious diel variations. Furthermore, NACs mainly originated from secondary formation in summer, whereas NACs at night were significantly contributed by BB and coal combustion in winter. Hence, we would focus on the diel variations and secondary formation pathways of NAC species during the summer campaign which was in the absence of other confounding sources.

For the NP subgroup, 2M4NP and DMNP presented daytime enhancements in summer (Figures 5b, 5c, 5k, and 5l), suggesting a significant source from photochemical formation. For nitrophenols, Yuan et al. (2016) showed that the gas-phase photooxidation of aromatics predominantly contributed to nitrophenols with the contribution from nighttime reaction of phenol with  $NO_3$  radicals relatively lower. However, 4NP herein did not show obvious daytime enhancement in summer, probably owing to the greater gas-particle partitioning at night or strong photolysis loss during the day. Yuan et al. (2016) predicted the photolysis loss rates of 17 ppt  $day^{-1}$  and lifetime of  $\sim 80$  min due to photolysis at noontime for nitrophenol, using the Master Chemical Mechanism box model. Photolysis has been recognized as a dominant sink for nitrophenol, but is less effective on MNP, the average photolysis rate of which is nearly one order of magnitude lower than that of nitrophenols (Bejan et al., 2007; Cheng et al., 2021). Additionally, there was a weak correlation between 4NP and  $NO_2$  ( $r = 0.47$ ) over the whole summer campaign (Table S6 in Supporting Information S1), whereas only a significant correlation at night ( $r = 0.86$ ) was observed when considering the diurnal and nocturnal environments separately (Table S7 in Supporting Information S1), which further suggested that photolysis was an efficient gas-phase loss pathway for nitrophenols. 4NP exhibited a good correlation ( $r = 0.55$ ) with benzene during daytime in summer, indicating the significance of photooxidation of benzene in 4NP formation. On the other hand, the ratios between the daytime

**Figure 5.** (a) Diel variations of (a) solar radiation ( $R_s$ ), (b) 2-Methyl-4-nitrophenol (2M4NP), (c) Dimethyl-nitrophenol (DMNP), (d) 4-Nitrocatechol (4NC), (f) 3-Methyl-5-nitrocatechol (3M5NC), (g) 3-Methyl-6-nitrocatechol (3M6NC), (h) 3-nitrosalicylic acid (3NSA), (i) 5-nitrosalicylic acid (5NSA), and (j) 3-hydroxy-5-nitrobenzoic acid (3H5NA) during the summer and winter. The relevant nitroaromatic compound (NAC) species exhibited daytime enhancements in summer. (b) Diel variations of (k) 4-nitrophenol (4NP), (l) 3-methyl-4-nitrophenol (3M4NP), (m) 4-methyl-5-nitrocatechol (4M5NC), and (n) 4-nitroguaiacol (4NG) in summer and winter campaigns. The day-night variations were not as obvious in summer. The daytime and nighttime samples are denoted by empty and solid marks, respectively. Note, the abundance of species from summer and winter campaigns refer to the left and right y axis, respectively. The pollution episodes are marked by light yellow shading.



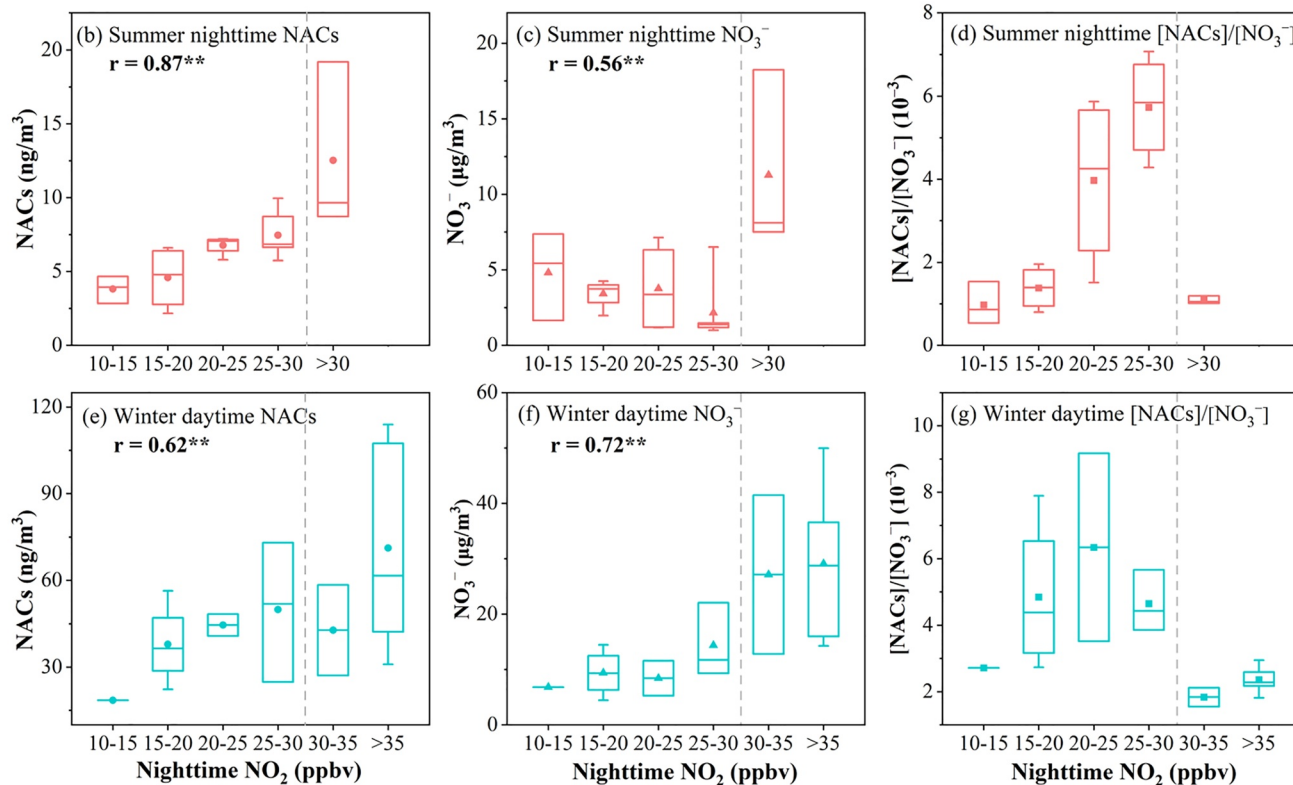
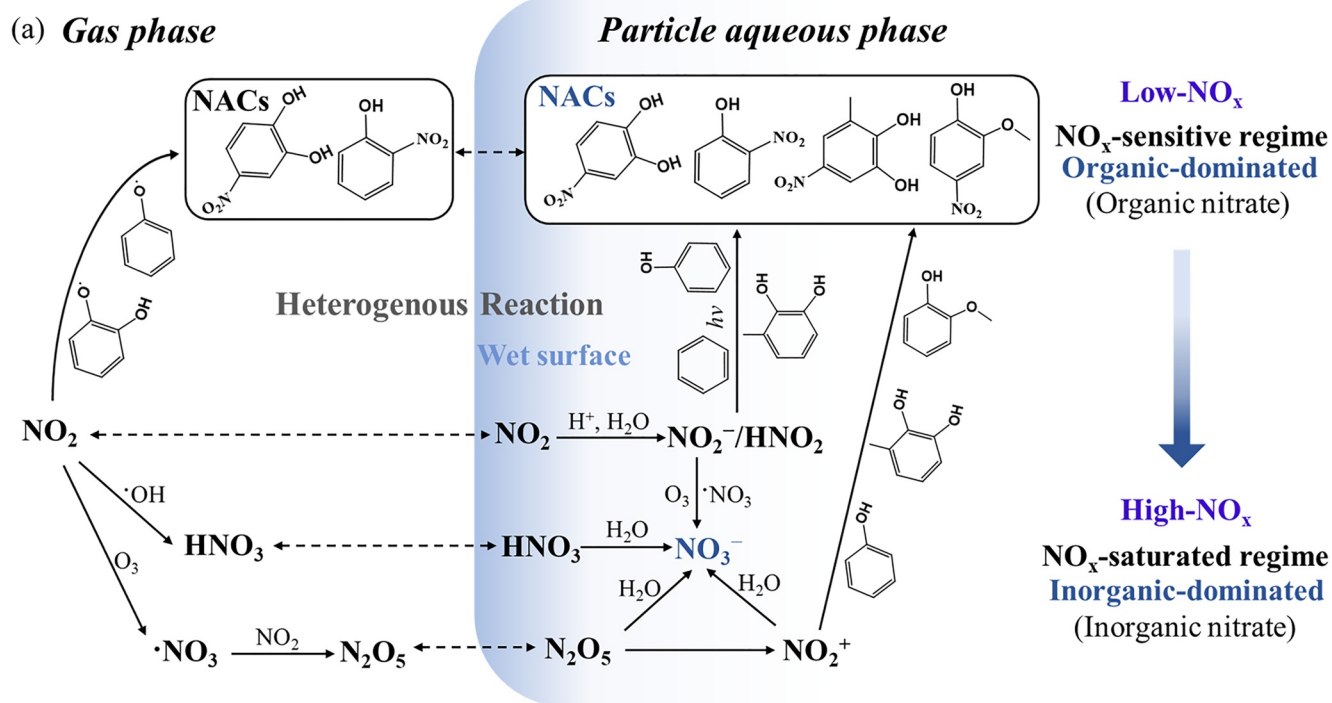


**Figure 6.** (a) Schematic description of the competitive formation pathways of nitroaromatic compounds (NACs) and inorganic nitrate (Bolzacchini et al., 2001; Edwards et al., 2017; Finewax et al., 2018; Frka et al., 2016; Harrison, Barra, et al., 2005; Harrison, Heal, & Cape, 2005; Heal et al., 2007; Kroflic et al., 2015; Vidovic et al., 2018; Vione et al., 2004). (b–g) Variations of NACs, nitrate concentrations and  $[\text{NACs}]/[\text{NO}_3^-]$  concentration ratios as a function of  $\text{NO}_2$  concentration bins (ppb) in the summer (pink, b–d) and winter (cyan, e–g) field campaigns. The closed markers within boxes represent the mean values, whiskers represent 1 and 99 percentiles, and the bottom and top of boxes represent 25 and 75 percentiles in each concentration bin. The  $r$  value in each panel represents the correlation coefficient between NACs or  $\text{NO}_3^-$  and nighttime  $\text{NO}_2$  concentrations. **\*\*** Correlation is significant at 0.01 (2-tailed).

and nighttime concentrations in summer for 4NP, 2M4NP, and DMNP were 1.12, 1.42, and 1.71 on average, respectively, suggesting that the substituted alkyl groups enhanced the diel variations in nitrated phenols, either through greater production or weaker loss during the day or through greater gas-particle partitioning at night. MNP and DMNP in summer also showed good correlations ( $r \geq 0.51$ ) with toluene and benzene during daytime. Moreover, 4NP, MNP, and DMNP in summer correlated poorly with atmospheric RH and were mainly in the gas phase (Table S4 in Supporting Information S1). These results indicated that gas-phase oxidation of aromatic VOCs might play a more significant role in the secondary formation of NP and its methylated derivatives than aqueous-phase and heterogeneous reactions.

Similar to 2M4NP and DMNP, 4NC, 3M5NC, and 3M6NC also showed daytime enhancements during the summer (Figures 5d, 5f and 5g), suggesting a significant contribution of photochemical reactions to secondary NCs. Previous studies showed that gas-phase oxidation of aromatic VOCs in the presence of  $\text{NO}_x$  (including photooxidation and nocturnal oxidation) was an important pathway to form atmospheric 4NC (Finewax et al., 2018; Lin et al., 2015; Xie et al., 2017), which was indicated by moderate to strong correlations between 4NC and benzene, toluene, or  $\text{NO}_2$  in summer. Furthermore, 4NC in summer correlated strongly with  $\text{O}_3$  ( $r = 0.58$ ) during daytime and weakly with atmospheric RH ( $r = -0.37$ ), which further underscored that the gas-phase photooxidation could be more important for 4NC formation. For MNC species, 4M5NC, 3M5NC, and 3M6NC inversely correlated with atmospheric RH in summer ( $|r| \geq 0.44$ , Table S6 in Supporting Information S1). Our observation was contrary to Wang et al.'s study (Y. Wang et al., 2019), where elevated ambient RH would promote the aqueous-phase formation of 4M5NC and 3M5NC. This appears reasonable because the average ambient RH in Shanghai (67% in summer, Figure 4a) was much higher than that in the summer of Beijing (37%) and increased RH would promote the water uptake of aerosols, ultimately leading to excessive ALWC and then increased pH through dilution. Recent studies have reported that aqueous-phase oxidation can be an important pathway for secondary MNC formation in the atmosphere, especially in polluted environments with high  $\text{NO}_x$  abundance and relatively acidic particles (pH around 3) (Vidovic et al., 2018, 2019, 2020; Y. Wang et al., 2019). In our summer campaign, the acidic particles exhibited higher pH under high RH conditions (pH = 4.3) than low RH conditions (pH = 2.9, Figure S11 in Supporting Information S1). Thus, MNC formation could decrease with higher RH (Figure S15 in Supporting Information S1,  $r = -0.53$ ), which was attributed to increased pH as a result of higher ALWC. This implied that aqueous-phase oxidation could represent an important pathway to form MNC. Here, the daytime enhancements of 3M5NC and 3M6NC in summer were likely attributed to stronger aqueous-phase oxidation as a result of lower pH during daytime. Quantum chemical calculations predicted the preferential formation of 3M5NC isomer via nighttime aqueous-phase electrophilic substitution and nitration of 3MC by  $\text{NO}_2^+$ , whereas the formation of 3M6NC was negligible because of the higher activation barrier for nitration of 3MC to form 3M6NC than 3M5NC (Frka et al., 2016). In this study, the levels of 3M5NC were generally higher than those of 3M6NC (Figure 3 and Figure S9 in Supporting Information S1), as theoretically predicted in Frka et al. (2016), where 3M5NC isomer dominated in ambient aerosols.

The daytime levels of 3NSA, 5NSA, and 3H5NA generally exceeded the nighttime ones in summer (Figures 5h–5j), indicating a preferential photooxidation formation of nitrosalicylic acids. This is in agreement with Ikemori et al.'s study (2019), where photooxidation is a dominant source of 3NSA and 5NSA. L. Wang et al. (2018) also indicated that NSAs were formed mostly from secondary formation that was dominated by  $\text{NO}_2$  nitration. 3NSA, 5NSA, and 3H5NA showed similar temporal variations (Figures 5h–5j) and strong correlations in summer, suggesting their similar formation behaviors or limiting factors. Furthermore, 3NSA, 5NSA, and 3H5NA correlated moderately to strongly with toluene ( $r \geq 0.52$ ) and  $\text{NO}_2$  ( $r \geq 0.48$ ) in summer, implying their possible secondary formation from oxidation of toluene in the presence of  $\text{NO}_2$ . 5NSA has been reported as a product by photooxidation of toluene in the presence of  $\text{NO}_x$  (Jang & Kamens, 2001), while the formation pathways of 3NSA and 3H5NA remain unclear. Clearly, more studies are needed to better understand the origins and formation mechanisms of anthropogenic NACs in polluted atmospheres.

### 3.4. Sensitivity of NAC Formation to $\text{NO}_2$ Abundance

As shown in Figure S1 of Supporting Information S1, in the presence of  $\text{NO}_2$ , NACs could be produced from OH or  $\text{NO}_3$  radical-induced oxidation of aromatic alcohols (e.g., phenol and cresol), which are the first oxidation products of benzene and toluene (Berndt & Böge, 2003; Finewax et al., 2018; Frka et al., 2016; Harrison, Heal, & Cape, 2005; Jenkin et al., 2003; Vione et al., 2004). For example, nitrophenol is generated from  $\text{NO}_2$  nitration

of phenoxy radical ( $C_6H_5O\bullet$ ), which is an intermediate arising from reaction of phenol with  $\bullet OH$  during the day or at night with  $NO_3\bullet$  (Berndt & Böge, 2003). Furthermore, the analysis in this work has suggested that the oxidation of aromatics by  $\bullet OH$  or  $NO_3\bullet$  in the presence of  $NO_x$  was an important source of NACs in Shanghai, especially in summer. The total quantified NACs and  $NO_2$  exhibited similar temporal variations (Figure 4) and showed good correlations ( $r = 0.54$  in summer and  $r = 0.68$  in winter) during the whole campaign. However, when daytime and nighttime  $NO_2$  were considered separately, only the nighttime samples showed a significant correlation ( $r \geq 0.74$ ) between NACs and  $NO_2$  (see in Tables S7 and S9 of Supporting Information S1) and the daytime samples exhibited no or lower correlation due to the influence from the daytime photolysis and decomposition of NACs (Bejan et al., 2007; Vione et al., 2009; Yuan et al., 2016). This might hint the significance of  $NO_3\bullet$ -initiated oxidation in NACs formation during nighttime, consistent with recent studies (X. R. Li et al., 2020; L. Wang et al., 2018).

To further elucidate the sensitivity of NAC secondary formation to  $NO_2$  abundance and understand the underlying atmospheric chemical processes, the concentrations of the total NACs and  $NO_3^-$  as well as the mass ratio of total NACs to  $NO_3^-$  (i.e.,  $[NACs]/[NO_3^-]$ ) as a function of  $NO_2$  abundance were plotted in Figure 6. Only data from nighttime samples in summer and daytime samples in winter were analyzed here in view of the stronger photolysis and decomposition of NACs during the day in summer and the importance of primary emission at night in winter. In general, higher levels of NACs and  $NO_3^-$  were observed with elevated  $NO_2$  abundance in box whisker plots in Figure 6b, 6c, 6e, and 6f. During the winter, under low- $NO_x$  environments ( $NO_2 < 30$  ppb), NACs apparently rose with  $NO_2$  increasing. Meanwhile, the  $NO_3^-$  levels were lower and  $[NACs]/[NO_3^-]$  ratios were higher. When  $NO_2$  rose to a level above 30 ppb, the NAC abundance did not further rise with  $NO_2$  increasing, hinting at a transition from  $NO_x$ -sensitive to  $NO_x$ -saturated regimes for secondary NAC formation. Meanwhile, the  $NO_3^-$  levels showed increasing trends while  $[NACs]/[NO_3^-]$  ratios decreased (Figures 6e–6g), which further indicated that the daytime  $NO_2$  was in excess for the  $NO_3\bullet$  oxidation and  $NO_2$  nitration of aromatic alcohols at  $NO_2 > 30$  ppb, and then the superfluous  $NO_2$  would be further oxidized to produce inorganic nitrate, resulting in a shift of products from organic-to inorganic-dominated conditions. Analogously, during summertime, a transition value was observed at  $NO_2 \sim 30$  ppb in which  $NO_x$  oxidation products were converted from organic to inorganic dominance (Figures 6b–6d). The summertime NAC formation still increased with  $NO_2$ , but  $[NACs]/[NO_3^-]$  ratios declined sharply and the  $NO_x$  oxidation products were dominated by inorganic nitrate under high- $NO_x$  environments ( $NO_2 > 30$  ppb). Higher  $[NACs]/[NO_3^-]$  mass ratios were observed under low- $NO_x$  environments, suggesting that a larger fraction of  $NO_2$  was transformed into organonitrogen when  $NO_2$  was less abundant. Figure 6a shows the schematic description of the competitive formation pathways of NACs and inorganic nitrate. Although both of the  $NO_2$  transition values in summer and winter were  $\sim 30$  ppb, the number of samples collected in  $NO_2 > 30$  ppb atmospheric environments (Figure 5) as well as the increasing ranges of particle-phase NACs and  $NO_3^-$  with  $NO_2$  during wintertime were much larger than the summertime one (Figure 6), which could be attributed to the higher concentrations of aromatics and  $NO_x$  (Figure 3 and Figure S8 in Supporting Information S1) and greater gas-particle partitioning in winter.

In the past decade, a clear decreasing trend in nitrate aerosols in China has emerged because of aggressive controls on  $NO_x$  emissions (Shen et al., 2020; Yan et al., 2020), and this trend will likely continue in the next several decades. Hence, the relative abundance of NACs and inorganic nitrate in China is expected to shift in favor of NACs, and organonitrogen would play a more important role in influencing aerosol properties, such as light absorptivity, hygroscopicity, surface tension, and toxicity (Moise et al., 2015; Ozel et al., 2011; Twohy et al., 2005).

We take the compositional variation of NACs and nitrate as an example for illustrating that the transition from low-to high- $NO_x$  regimes and the corresponding  $NO_x$  oxidation products shifting from organic-to inorganic-dominated conditions exist in polluted urban atmospheres that are characterized by high  $NO_x$  and anthropogenic VOCs. However, compared with the well-known BVOC- $NO_x$  atmospheres (Edwards et al., 2017), the mechanisms and transition thresholds for anthropogenic VOCs- $NO_x$  atmospheres were less elucidated. In this study, the  $NO_x$  regime transition value was expressed by  $NO_2$  concentrations instead of  $NO_2/VOCs$  or  $NO_x/VOCs$  ratios due to only a limited number of quantified VOC species. Note that the  $NO_x$  regime transition values could vary in different atmospheric conditions. Clearly, further comprehensive investigation through laboratory simulation and field observations are warranted for developing more quantitative understanding of the  $NO_x$  regime transition for anthropogenic VOCs- $NO_x$  under various atmospheric environments.

### 3.5. Effects of Other Factors on NAC Formation

Nitration of aromatic hydrocarbons (e.g., benzene and toluene) represented an important source of NACs in urban Shanghai, especially in summer. Overall, a rise in NAC abundance was found with benzene and toluene increasing during the summer and winter (Figures S12 and S13 in Supporting Information S1), but the summer abundance of NACs appeared much lower and the increase was less prominent than the winter concentrations. This is expected because during wintertime locally there were more BB activities ( $K^+$ , Figure 4) and substantial pollutants (e.g., NACs, benzene, toluene, and  $NO_x$ ) transported from elsewhere in the heating regions (Figure S16 in Supporting Information S1). During summertime, when benzene and toluene were higher than 0.8 and 2.2 ppb, respectively, the daytime NAC levels did not further increase discernibly with benzene and toluene increasing (Figures S12a and S13a in Supporting Information S1), indicating that benzene and toluene were excessively present, and thereby ceased to be the limiting factors for secondary NAC formation. Likewise, the nocturnal NAC formation would become independent of these precursors with benzene and toluene higher than 0.6 and 2.2 ppb, respectively. In addition, compared with summer, the transition values of benzene and toluene in winter were higher, reaching 1.2 and 4.2 ppb, respectively, likely owing to the significantly higher  $NO_x$  abundance with higher oxidation capacity to VOC precursors in winter.

The total NACs showed no apparent correlations with  $O_3$  in summer and winter (Tables S6 and S8 in Supporting Information S1). However, when considering the daytime and nighttime conditions separately, only 4NC and 3M5NC showed strong positive correlations with  $O_3$  during daytime in summer, whereas individual NAC species were greatly correlated with  $O_3$  during daytime and they at night were largely anticorrelated with  $O_3$  during the winter (Tables S7 and S9, Figure S15 in Supporting Information S1), implying that the formation pathways of NACs could vary under different atmospheric conditions. Recent studies have suggested that during daytime, oxidation by OH radicals (mainly generated from the photochemical process of  $O_3$ ) dominates secondary formation of NAC, while oxidation by  $NO_3$  radicals (mostly formed by reaction of  $O_3$  with  $NO_2$ ) accounts for the nighttime formation (Finewax et al., 2018; C. Li et al., 2020; X. R. Li et al., 2020). Moreover, the high  $O_3$  abundance indicated strong photochemistry. Among our summer and winter campaigns, the level of  $O_3$  reduced in the following order: (daytime, summer) > (nighttime, summer) or (daytime, winter) > (nighttime, winter) (Figure S8 in Supporting Information S1). This abundance order was likely impelled by solar radiation intensity. During daytime in summer, 4NP and MNP poorly correlated with  $O_3$ , probably attributable to their stronger photolysis than 4NC and MNC. It is thereby possible that stronger photochemistry involving  $O_3$  led to higher concentrations of 4NC and 3M5NC during daytime in summer. During nighttime in winter, the low  $O_3$  could constantly oxidize  $NO_2$  to form  $NO_3$  and the nighttime formation of NACs was dominated by  $NO_3$ -initiated oxidation, ultimately resulting in lower  $O_3$  and higher NAC abundance. Nevertheless, no apparent correlation was found between NACs and  $O_3$  in the nighttime of summer and daytime of winter (Tables S7 and S9 in Supporting Information S1). This appears to suggest that the  $O_3$  oxidant level only acted as a limiting factor to NAC abundance in certain conditions. More field observations and comprehensive lab simulations are required to gain a reasonable explanation.

Previous studies have reported that the semi-volatile characteristics of NACs would lead to a temperature-dependent partitioning between gas- and particle-phases, especially for NPs (Al-Naiema & Stone, 2017; Cecinato et al., 2005), which was also verified in this work (discussed in Section 3.2.2). Based on the linear correlations between the three subgroups and temperature shown in Figure S14 of Supporting Information S1, three kinds of NAC subgroups were differently dependent on temperature throughout the entire sampling periods: the concentrations of NPs showed the strongest dependence. This observation indicated that NPs possessed greater volatility than NCs or NSAs. It is therefore possible that the aqueous/particle-phase NPs would be more prone to be evaporated or lost from the aerosols in higher ambient temperatures via enhanced transfer into the gas phase or via increased photolysis than NCs or NSAs.

In summary, anthropogenic emissions have a great effect on the formation of NACs in urban Shanghai. The total number and abundance of NACs could increase significantly in polluted air, especially in winter. Our results advance the understanding of NAC formation in polluted atmospheres, and highlight the importance of reducing anthropogenic pollutant emissions, especially anthropogenic VOCs and  $NO_x$ , to reduce the toxic organic aerosol burden in urban areas. Future field studies combined with chamber experiments and model simulations are warranted for achieving an integral understanding of the production and losses of NACs in polluted urban environments.



## Conflict of Interest

The authors declare no conflicts of interest relevant to this study.

## Data Availability Statement

The meteorological data were obtained from the Gridded Meteorological Data Archives of the Air Resources Laboratory (<https://ready.arl.noaa.gov/archives.php>) (ARL, 2022). HYSPLIT provided the air mass reanalysis data (<http://www.arl.noaa.gov/ready/hysplit4.html>) (Rolph et al., 2017). The chromatogram-mass spectrometry data were processed with MZmine version 2.30 (Hu et al., 2016; X. Wang et al., 2020), available under the MZmine license at <http://mzmine.github.io/>. Additional data generated in this manuscript could be downloaded at Mendeley (<https://data.mendeley.com/datasets/3zry3kfyf2/1>) (Cai, 2022).

## Acknowledgments

This work was supported by the National Natural Science Foundation of China (No. 42061134006, 21876029, and 42175179) and Science & Technology Commission of Shanghai Municipality (No. 21DZ1202300).

## References

- Al-Naiema, I. M., & Stone, E. A. (2017). Evaluation of anthropogenic secondary organic aerosol tracers from aromatic hydrocarbons. *Atmospheric Chemistry and Physics*, 17(3), 2053–2065. <https://doi.org/10.5194/acp-17-2053-2017>
- ARL (2022). Gridded meteorological data archives of the air resources laboratory [Dataset]. NOAA. <https://ready.arl.noaa.gov/archives.php>
- Atkinson, R., Aschmann, S. M., & Arey, J. (1992). Reactions of hydroxyl and nitrogen trioxide radicals with phenol, cresols, and 2-nitrophenol at 296 ± 2 K. *Environmental Science & Technology*, 26(7), 1397–1403. <https://doi.org/10.1021/es00031a018>
- Bannan, T. J., Booth, A. M., Jones, B. T., O'Meara, S., Barley, M. H., Riipinen, I., et al. (2017). Measured saturation vapor pressures of phenolic and nitro-aromatic compounds. *Environmental Science & Technology*, 51(7), 3922–3928. <https://doi.org/10.1021/acs.est.6b06364>
- Bejan, I., Barnes, I., Olariu, R., Zhou, S., Wiesen, P., & Benter, T. (2007). Investigations on the gas-phase photolysis and OH radical kinetics of methyl-2-nitrophenols. *Physical Chemistry Chemical Physics*, 9(42), 5686–5692. <https://doi.org/10.1039/b709464g>
- Bejan, I., Duncianu, M., Olariu, R., Barnes, I., Seakins, P. W., & Wiesen, P. (2015). Kinetic study of the gas-phase reactions of chlorine atoms with 2-chlorophenol, 2-nitrophenol, and four methyl-2-nitrophenol isomers. *Journal of Physical Chemistry A*, 119(20), 4735–4745. <https://doi.org/10.1021/acs.jpca.5b02392>
- Berndt, T., & Böge, O. (2003). Gas-phase reaction of OH radicals with phenol. *Physical Chemistry Chemical Physics*, 5(2), 342–350. <https://doi.org/10.1039/b208187c>
- Bolzacchini, E., Bruschi, M., Hjorth, J., Meinardi, S., Orlandi, M., Rindone, B., & Rosenbohm, E. (2001). Gas-phase reaction of phenol with NO<sub>3</sub>. *Environmental Science & Technology*, 35(9), 1791–1797. <https://doi.org/10.1021/es001290m>
- Cai, D. (2022). Data: Formation of secondary nitroaromatic compounds in polluted urban environments [Dataset]. Mendeley. <https://data.mendeley.com/datasets/3zry3kfyf2/1>
- Cai, D., Wang, X., Chen, J., & Li, X. (2020). Molecular characterization of organosulfates in highly polluted atmosphere using ultra-high-resolution mass spectrometry. *Journal of Geophysical Research: Atmospheres*, 125(8). <https://doi.org/10.1029/2019jd032253>
- Cecinato, A., Di Palo, V., Pomata, D., Sciano, M. C. T., & Possanzini, M. (2005). Measurement of phase-distributed nitrophenols in Rome ambient air. *Chemosphere*, 59(5), 679–683. <https://doi.org/10.1016/j.chemosphere.2004.10.045>
- Chen, Y., Zheng, P., Wang, Z., Pu, W., Tan, Y., Yu, C., et al. (2021). Secondary formation and impacts of gaseous nitro-phenolic compounds in the continental outflow observed at a background site in South China. *Environmental Science & Technology*. <https://doi.org/10.1021/acs.est.1c04596>
- Cheng, X., Chen, Q., Li, Y., Huang, G., Liu, Y., Lu, S., et al. (2021). Secondary production of gaseous nitrated phenols in polluted urban environments. *Environmental Science & Technology*. <https://doi.org/10.1021/acs.est.0c07988>
- Chow, K. S., Huang, X. H. H., & Yu, J. Z. (2016). Quantification of nitroaromatic compounds in atmospheric fine particulate matter in Hong Kong over 3 years: Field measurement evidence for secondary formation derived from biomass burning emissions. *Environmental Chemistry*, 13(4), 665. <https://doi.org/10.1071/en15174>
- Donahue, N. M., Robinson, A. L., Stanier, C. O., & Pandis, S. N. (2006). Coupled partitioning, dilution, and chemical aging of semivolatile organics. *Environmental Science & Technology*, 40(8), 2635–2643. <https://doi.org/10.1021/es052297c>
- Draxier, R. R., & Hess, G. D. (1998). An overview of the HYSPLIT\_4 modelling system for trajectories, dispersion and deposition. *Australian Meteorological Magazine*, 47(4), 295–308.
- Edwards, P. M., Aikin, K. C., Dube, W. P., Fry, J. L., Gilman, J. B., de Gouw, J. A., et al. (2017). Transition from high- to low-NO<sub>x</sub> control of night-time oxidation in the southeastern US. *Nature Geoscience*, 10(7), 490–495. <https://doi.org/10.1038/ngeo2976>
- Fernandez, P., Grifoll, M., Solanas, A. M., Bayona, J. M., & Albaiges, J. (1992). Bioassay-directed chemical-analysis of genotoxic components in coastal sediments. *Environmental Science & Technology*, 26(4), 817–829. <https://doi.org/10.1021/es00028a024>
- Finewax, Z., de Gouw, J. A., & Ziemann, P. J. (2018). Identification and quantification of 4-Nitrocatechol formed from OH and NO<sub>3</sub> radical-initiated reactions of catechol in Air in the presence of NO<sub>x</sub>: Implications for secondary organic aerosol formation from biomass burning. *Environmental Science & Technology*, 52(4), 1981–1989. <https://doi.org/10.1021/acs.est.7b05864>
- Frka, S., Sala, M., Kroflic, A., Hus, M., Cusak, A., & Grdic, I. (2016). Quantum chemical calculations resolved identification of methylnitrocatechols in atmospheric aerosols. *Environmental Science & Technology*, 50(11), 5526–5535. <https://doi.org/10.1021/acs.est.6b00823>
- Gao, Y., Wang, H., Zhang, X., Jing, S. a., Peng, Y., Qiao, L., et al. (2019). Estimating secondary organic aerosol production from toluene photochemistry in a megacity of China. *Environmental Science & Technology*, 53(15), 8664–8671. <https://doi.org/10.1021/acs.est.9b00651>
- Grundlingh, J., Dargan, P. I., El-Zanfaly, M., & Wood, D. M. (2011). 2,4-dinitrophenol (DNP): A weight loss agent with significant acute toxicity and risk of death. *Journal of Medical*, 7(3), 205–212. <https://doi.org/10.1007/s13181-011-0162-6>
- Harrison, M. A. J., Barra, S., Borghesi, D., Vione, D., Arsene, C., & Olariu, R. L. (2005). Nitrated phenols in the atmosphere: A review. *Atmospheric Environment*, 39(2), 231–248. <https://doi.org/10.1016/j.atmosenv.2004.09.044>
- Harrison, M. A. J., Heal, M. R., & Cape, J. N. (2005). Evaluation of the pathways of tropospheric nitrophenol formation from benzene and phenol using a multiphase model. *Atmospheric Chemistry and Physics*, 5(6), 1679–1695. <https://doi.org/10.5194/acp-5-1679-2005>
- Heal, M. R., Harrison, M. A. J., & Cape, J. N. (2007). Aqueous-phase nitration of phenol by N<sub>2</sub>O<sub>5</sub> and ClNO<sub>2</sub>. *Atmospheric Environment*, 41(17), 3515–3520. <https://doi.org/10.1016/j.atmosenv.2007.02.003>



- Hu, M., Krauss, M., Brack, W., & Schulze, T. (2016). Optimization of LC-Orbitrap-HRMS acquisition and MZmine 2 data processing for nontarget screening of environmental samples using design of experiments. *Analytical and Bioanalytical Chemistry*, 408(28), 7905–7915. <https://doi.org/10.1007/s00216-016-9919-8>
- Huang, Q. G., Wang, L. S., & Han, S. K. (1995). The genotoxicity of substituted nitrobenzenes and the quantitative structure-activity relationship studies. *Chemosphere*, 30(5), 915–923. [https://doi.org/10.1016/0045-6535\(94\)00450-9](https://doi.org/10.1016/0045-6535(94)00450-9)
- Huang, R. J., Zhang, Y., Bozzetti, C., Ho, K. F., Cao, J. J., Han, Y., et al. (2014). High secondary aerosol contribution to particulate pollution during haze events in China. *Nature*, 514(7521), 218–222. <https://doi.org/10.1038/nature13774>
- Hughey, C. A., Hendrickson, C. L., Rodgers, R. P., Marshall, A. G., & Qian, K. N. (2001). Kendrick mass defect spectrum: A compact visual analysis for ultrahigh-resolution broadband mass spectra. *Analytical Chemistry*, 73(19), 4676–4681. <https://doi.org/10.1021/ac010560w>
- Iinuma, Y., Boege, O., Graefe, R., & Herrmann, H. (2010). Methyl-nitrocatechols: Atmospheric tracer compounds for biomass burning secondary organic aerosols. *Environmental Science & Technology*, 44(22), 8453–8459. <https://doi.org/10.1021/es102938a>
- Ikemori, F., Nakayama, T., & Hasegawa, H. (2019). Characterization and possible sources of nitrated mono- and di-aromatic hydrocarbons containing hydroxyl and/or carboxyl functional groups in ambient particles in Nagoya, Japan. *Atmospheric Environment*, 211(AUG), 91–102. <https://doi.org/10.1016/j.atmosenv.2019.05.009>
- Jang, M. S., & Kamens, R. M. (2001). Characterization of secondary aerosol from the photooxidation of toluene in the presence of NO<sub>x</sub> and 1-propene. *Environmental Science & Technology*, 35(18), 3626–3639. <https://doi.org/10.1021/es010676+>
- Jenkin, M. E., Saunders, S. M., Wagner, V., & Pilling, M. J. (2003). Protocol for the development of the Master Chemical Mechanism, MCM v3 (Part B): Tropospheric degradation of aromatic volatile organic compounds. *Atmospheric Chemistry and Physics*, 3(1), 181–193. <https://doi.org/10.5194/acp-3-181-2003>
- Kahnt, A., Behrouzi, S., Vermeylen, R., Shalamzari, M. S., Vercauteren, J., Roekens, E., et al. (2013). One-year study of nitro-organic compounds and their relation to wood burning in PM<sub>10</sub> aerosol from a rural site in Belgium. *Atmospheric Environment*, 81, 561–568. <https://doi.org/10.1016/j.atmosenv.2013.09.041>
- Kelly, J. L., Michelangeli, D. V., Makar, P. A., Hastie, D. R., Mozurkewich, M., & Auld, J. (2010). Aerosol speciation and mass prediction from toluene oxidation under high NO<sub>x</sub> conditions. *Atmospheric Environment*, 44(3), 361–369. <https://doi.org/10.1016/j.atmosenv.2009.10.035>
- Kim, S., Kramer, R. W., & Hatcher, P. G. (2003). Graphical method for analysis of ultrahigh-resolution broadband mass spectra of natural organic matter, the van Krevelen diagram. *Analytical Chemistry*, 75(20), 5336–5344. <https://doi.org/10.1021/ac034415p>
- Kitanovski, Z., Grgic, I., Vermeylen, R., Claeys, M., & Maenhaut, W. (2012). Liquid chromatography tandem mass spectrometry method for characterization of monoaromatic nitro-compounds in atmospheric particulate matter. *Journal of Chromatography A*, 1268, 35–43. <https://doi.org/10.1016/j.chroma.2012.10.021>
- Kitanovski, Z., Hovorka, J., Kuta, J., Leoni, C., Prokes, R., Sanka, O., et al. (2020). Nitrated monoaromatic hydrocarbons (nitrophenols, nitrocatechols, nitrosalicylic acids) in ambient air: Levels, mass size distributions and inhalation bioaccessibility. *Environmental Science and Pollution Research*.
- Kitanovski, Z., Shahpoury, P., Samara, C., Voliotis, A., & Lammel, G. (2020). Composition and mass size distribution of nitrated and oxygenated aromatic compounds in ambient particulate matter from southern and central Europe—Implications for the origin. *Atmospheric Chemistry and Physics*, 20(4), 2471–2487. <https://doi.org/10.5194/acp-20-2471-2020>
- Kourtchev, I., Fuller, S., Aalto, J., Ruuskanen, T. M., McLeod, M. W., Maenhaut, W., et al. (2013). Molecular composition of boreal forest aerosol from Hyttiala, Finland, using ultrahigh resolution mass spectrometry. *Environmental Science & Technology*, 47(9), 4069–4079. <https://doi.org/10.1021/es3051636>
- Krofflic, A., Grlic, M., & Grgic, I. (2015). Unraveling pathways of guaiacol nitration in atmospheric waters: Nitrite, a source of reactive nitronium ion in the atmosphere. *Environmental Science & Technology*, 49(15), 9150–9158. <https://doi.org/10.1021/acs.est.5b01811>
- Krofflic, A., Hus, M., Grlic, M., & Grgic, I. (2018). Underappreciated and complex role of nitrous acid in aromatic nitration under mild environmental conditions: The case of activated methoxyphenols. *Environmental Science & Technology*, 52(23), 13756–13765. <https://doi.org/10.1021/acs.est.8b01903>
- Laskin, A., Laskin, J., & Nizkorodov, S. A. (2015). Chemistry of atmospheric brown carbon. *Chemical Reviews*, 115(10), 4335–4382. <https://doi.org/10.1021/cr5006167>
- Laskin, A., Smith, J. S., & Laskin, J. (2009). Molecular characterization of nitrogen-containing organic compounds in biomass burning aerosols using high-resolution mass spectrometry. *Environmental Science & Technology*, 43(10), 3764–3771. <https://doi.org/10.1021/es803456n>
- Lauraguais, A., Coeur-Tourneur, C., Cassez, A., Deboudt, K., Fourmentin, M., & Choel, M. (2014). Atmospheric reactivity of hydroxyl radicals with guaiacol (2-methoxyphenol), a biomass burning emitted compound: Secondary organic aerosol formation and gas-phase oxidation products. *Atmospheric Environment*, 86, 155–163. <https://doi.org/10.1016/j.atmosenv.2013.11.074>
- Le Breton, M., Wang, Y. J., Hallquist, A. M., Pathak, R. K., Zheng, J., Yang, Y. D., et al. (2018). Online gas- and particle-phase measurements of organosulfates, organosulfonates and nitrooxy organosulfates in Beijing utilizing a FIGAERO ToF-CIMS. *Atmospheric Chemistry and Physics*, 18(14), 10355–10371. <https://doi.org/10.5194/acp-2017-814>
- Li, C., He, Q., Fang, Z., Brown, S. S., Laskin, A., Cohen, S. R., & Rudich, Y. (2020). Laboratory insights into the diel cycle of optical and chemical transformations of biomass burning brown carbon aerosols. *Environmental Science & Technology*, 54(19), 11827–11837. <https://doi.org/10.1021/acs.est.0c04310>
- Li, K., Li, J., Tong, S., Wang, W., Huang, R.-J., & Ge, M. (2019). Characteristics of wintertime VOCs in suburban and urban Beijing: Concentrations, emission ratios, and festival effects. *Atmospheric Chemistry and Physics*, 19(12), 8021–8036. <https://doi.org/10.5194/acp-19-8021-2019>
- Li, M., Wang, X. F., Lu, C. Y., Li, R., Zhang, J., Dong, S. W., et al. (2020). Nitrated phenols and the phenolic precursors in the atmosphere in urban Jinan, China. *The Science of the Total Environment*, 714, 136760. <https://doi.org/10.1016/j.scitotenv.2020.136760>
- Li, X., Wang, Y., Hu, M., Tan, T., Li, M., Wu, Z., et al. (2020). Characterizing chemical composition and light absorption of nitroaromatic compounds in the winter of Beijing. *Atmospheric Environment*, 237, 117712. <https://doi.org/10.1016/j.atmosenv.2020.117712>
- Li, X. R., Yang, Y., Liu, S. Q., Zhao, Q., Wang, G. H., & Wang, Y. S. (2020). Light absorption properties of brown carbon (BrC) in autumn and winter in Beijing: Composition, formation and contribution of nitrated aromatic compounds. *Atmospheric Environment*, 223, 117289. <https://doi.org/10.1016/j.atmosenv.2020.117289>
- Liang, Y. H., Wang, X. F., Dong, S. W., Liu, Z. Y., Mu, J. S., Lu, C. Y., et al. (2020). Size distributions of nitrated phenols in winter at a coastal site in north China and the impacts from primary sources and secondary formation. *Chemosphere*, 250, 126256. <https://doi.org/10.1016/j.chemosphere.2020.126256>
- Lin, P., Bluvstein, N., Rudich, Y., Nizkorodov, S. A., Laskin, J., & Laskin, A. (2017). Molecular chemistry of atmospheric brown carbon inferred from a nationwide biomass burning event. *Environmental Science & Technology*, 51(20), 11561–11570. <https://doi.org/10.1021/acs.est.7b02276>

- Lin, P., Liu, J., Shilling, J. E., Kathmann, S. M., Laskin, J., & Laskin, A. (2015). Molecular characterization of brown carbon (BrC) chromophores in secondary organic aerosol generated from photo-oxidation of toluene. *Physical Chemistry Chemical Physics*, *17*(36), 23312–23325. <https://doi.org/10.1039/c5cp02563j>
- Lin, P., Rincon, A. G., Kalberer, M., & Yu, J. Z. (2012). Elemental composition of HULIS in the Pearl River Delta Region, China: Results inferred from positive and negative electrospray high resolution mass spectrometric data. *Environmental Science & Technology*, *46*(14), 7454–7462. <https://doi.org/10.1021/es300285d>
- Mohr, C., Lopez-Hilfiker, F. D., Zotter, P., Prevot, A. S., Xu, L., Ng, N. L., et al. (2013). Contribution of nitrated phenols to wood burning brown carbon light absorption in Detling, United Kingdom during winter time. *Environmental Science & Technology*, *47*(12), 6316–6324. <https://doi.org/10.1021/es400683v>
- Moise, T., Flores, J. M., & Rudich, Y. (2015). Optical properties of secondary organic aerosols and their changes by chemical processes. *Chemical Reviews*, *115*(10), 4400–4439. <https://doi.org/10.1021/cr5005259>
- Nannoolal, Y., Rarey, J., & Ramjugernath, D. (2008). Estimation of pure component properties - Part 3. Estimation of the vapor pressure of non-electrolyte organic compounds via group contributions and group interactions. *Fluid Phase Equilibria*, *269*(1–2), 117–133. <https://doi.org/10.1016/j.fluid.2008.04.020>
- O'Brien, R. E., Laskin, A., Laskin, J., Rubitschun, C. L., Surratt, J. D., & Goldstein, A. H. (2014). Molecular characterization of S- and N-containing organic constituents in ambient aerosols by negative ion mode high-resolution nanospray desorption electrospray ionization mass spectrometry: CalNex 2010 field study. *Journal of Geophysical Research: Atmospheres*, *119*(22), 12706–12720. <https://doi.org/10.1002/2014jd021955>
- Olariu, R. I., Klotz, B., Barnes, I., Becker, K. H., & Mocanu, R. (2002). FT-IR study of the ring-retaining products from the reaction of OH radicals with phenol, o-m- and p-cresol. *Atmospheric Environment*, *36*(22), 3685–3697. [https://doi.org/10.1016/s1352-2310\(02\)00202-9](https://doi.org/10.1016/s1352-2310(02)00202-9)
- Ozel, M. Z., Hamilton, J. F., & Lewis, A. C. (2011). New sensitive and quantitative analysis method for organic nitrogen compounds in urban aerosol samples. *Environmental Science & Technology*, *45*(4), 1497–1505. <https://doi.org/10.1021/es102528g>
- Pankow, J. F. (1994a). An absorption-model of the gas aerosol partitioning involved in the formation of secondary organic aerosol. *Atmospheric Environment*, *28*(2), 189–193. [https://doi.org/10.1016/1352-2310\(94\)90094-9](https://doi.org/10.1016/1352-2310(94)90094-9)
- Pankow, J. F. (1994b). An absorption model of gas/particle partitioning of organic compounds in the atmosphere. *Atmospheric Environment*, *28*(2), 185–188. [https://doi.org/10.1016/1352-2310\(94\)90093-0](https://doi.org/10.1016/1352-2310(94)90093-0)
- Pankow, J. F., Seinfeld, J. H., Asher, W. E., & Erdakos, G. B. (2001). Modeling the formation of secondary organic aerosol. I. Application of theoretical principles to measurements obtained in the  $\alpha$ -Pinene/,  $\beta$ -Pinene/, Sabinene/,  $\Delta$ 3-Carene/, and cyclohexene/ozone systems. *Environmental Science & Technology*, *35*(6), 1164–1172. <https://doi.org/10.1021/es001321d>
- Purohit, V., & Basu, A. K. (2000). Mutagenicity of nitroaromatic compounds. *Chemical Research in Toxicology*, *13*(8), 673–692. <https://doi.org/10.1021/tx000002x>
- Rolph, G., Stein, A., & Stunder, B. (2017). Real-time environmental applications and display system: READY. *Environmental Modelling & Software*, *95*, 210–228. <https://doi.org/10.1016/j.envsoft.2017.06.025>
- Salvador, C. M. G., Tang, R., Priestley, M., Li, L., Tsiligiannis, E., Le Breton, M., et al. (2021). Ambient nitro-aromatic compounds - Biomass burning versus secondary formation in rural China. *Atmospheric Chemistry and Physics*, *21*(3), 1389–1406. <https://doi.org/10.5194/acp-21-1389-2021>
- Sander, R. (2015). Compilation of Henry's law constants (version 4.0) for water as solvent. *Atmospheric Chemistry and Physics*, *15*(8), 4399–4981. <https://doi.org/10.5194/acp-15-4399-2015>
- Sato, K., Hatakeyama, S., & Imamura, T. (2007). Secondary organic aerosol formation during the photooxidation of toluene: NO<sub>x</sub> dependence of chemical composition. *Journal of Physical Chemistry A*, *111*(39), 9796–9808. <https://doi.org/10.1021/jp071419f>
- Shen, J. Y., Zhao, Q. B., Cheng, Z., Wang, P., Ying, Q., Liu, J., et al. (2020). Insights into source origins and formation mechanisms of nitrate during winter haze episodes in the Yangtze River Delta. *Science of the Total Environment*, *741*, 140187. <https://doi.org/10.1016/j.scitotenv.2020.140187>
- Slade, J. H., & Knopf, D. A. (2014). Multiphase OH oxidation kinetics of organic aerosol: The role of particle phase state and relative humidity. *Geophysical Research Letters*, *41*(14), 5297–5306. <https://doi.org/10.1002/2014gl060582>
- Song, J., Li, M., Fan, X., Zou, C., Zhu, M., Jiang, B., et al. (2019). Molecular characterization of water- and methanol-soluble organic compounds emitted from residential coal combustion using ultrahigh-resolution electrospray ionization Fourier transform ion cyclotron resonance mass spectrometry. *Environmental Science & Technology*, *53*(23), 13607–13617. <https://doi.org/10.1021/acs.est.9b04331>
- Song, J., Li, M., Jiang, B., Wei, S., Fan, X., & Peng, P. (2018). Molecular characterization of water-soluble humic like substances in smoke particles emitted from combustion of biomass materials and coal using ultrahigh-resolution electrospray ionization Fourier transform ion cyclotron resonance mass spectrometry. *Environmental Science & Technology*, *52*(5), 2575–2585. <https://doi.org/10.1021/acs.est.7b06126>
- Teich, M., van Pinxteren, D., Wang, M., Kecorius, S., Wang, Z. B., Muller, T., et al. (2017). Contributions of nitrated aromatic compounds to the light absorption of water-soluble and particulate brown carbon in different atmospheric environments in Germany and China. *Atmospheric Chemistry and Physics*, *17*(3), 1653–1672. <https://doi.org/10.5194/acp-17-1653-2017>
- Twohy, C. H., Anderson, J. R., & Crozier, P. A. (2005). Nitrogenated organic aerosols as cloud condensation nuclei. *Geophysical Research Letters*, *32*(19). <https://doi.org/10.1029/2005gl023605>
- Vidovic, K., Jurkovic, D. L., Sala, M., Krofflic, A., & Grgic, I. (2018). Nighttime aqueous-phase formation of nitrocatechols in the atmospheric condensed phase. *Environmental Science & Technology*, *52*(17), 9722–9730. <https://doi.org/10.1021/acs.est.8b01161>
- Vidovic, K., Krofflic, A., Jovanovic, P., Sala, M., & Grgic, I. (2019). Electrochemistry as a tool for studies of complex reaction mechanisms: The case of the atmospheric aqueous-phase aging of catechols. *Environmental Science & Technology*, *53*(19), 11195–11203. <https://doi.org/10.1021/acs.est.9b02456>
- Vidovic, K., Krofflic, A., Sala, M., & Grgic, I. (2020). Aqueous-phase brown carbon formation from aromatic precursors under sunlight conditions. *Atmosphere*, *11*(2), 131. <https://doi.org/10.3390/atmos11020131>
- Vione, D., Maurino, V., Minero, C., Duncianu, M., Olariu, R.-I., Arsene, C., et al. (2009). Assessing the transformation kinetics of 2- and 4-nitrophenol in the atmospheric aqueous phase. Implications for the distribution of both nitroisomers in the atmosphere. *Atmospheric Environment*, *43*(14), 2321–2327. <https://doi.org/10.1016/j.atmosenv.2009.01.025>
- Vione, D., Maurino, V., Minero, C., Lucchiari, M., & Pelizzetti, E. (2004). Nitration and hydroxylation of benzene in the presence of nitrite/nitrous acid in aqueous solution. *Chemosphere*, *56*(11), 1049–1059. <https://doi.org/10.1016/j.chemosphere.2004.05.027>
- Vione, D., Maurino, V., Minero, C., & Pelizzetti, E. (2001). Phenol photolysis upon UV irradiation of nitrite in aqueous solution I: Effects of oxygen and 2-propanol. *Chemosphere*, *45*(6–7), 893–902. [https://doi.org/10.1016/s0045-6535\(01\)00035-2](https://doi.org/10.1016/s0045-6535(01)00035-2)
- Wang, H., Lu, K., Guo, S., Wu, Z., Shang, D., Tan, Z., et al. (2018). Efficient N<sub>2</sub>O<sub>5</sub> uptake and NO<sub>3</sub> oxidation in the outflow of urban Beijing. *Atmospheric Chemistry and Physics*, *18*(13), 9705–9721. <https://doi.org/10.5194/acp-18-9705-2018>

- Wang, L., Wang, X., Gu, R., Wang, H., Yao, L., Wen, L., et al. (2018). Observations of fine particulate nitrated phenols in four sites in northern China: Concentrations, source apportionment, and secondary formation. *Atmospheric Chemistry and Physics*, 18(6), 4349–4359. <https://doi.org/10.5194/acp-18-4349-2018>
- Wang, X., Hayeck, N., Brüggemann, M., Abis, L., Riva, M., Lu, Y., et al. (2020). Chemical characteristics and brown carbon chromophores of atmospheric organic aerosols over the Yangtze River channel: A cruise campaign. *Journal of Geophysical Research: Atmospheres*, 125(16), e2020JD032497. <https://doi.org/10.1029/2020jd032497>
- Wang, X., Hayeck, N., Brüggemann, M., Yao, L., Chen, H., Zhang, C., et al. (2017). Chemical characteristics of organic aerosols in Shanghai: A study by ultrahigh-performance liquid chromatography coupled with Orbitrap mass spectrometry. *Journal of Geophysical Research: Atmospheres*, 122(21), 11703–11722. <https://doi.org/10.1002/2017jd026930>
- Wang, Y., Hu, M., Wang, Y., Zheng, J., Shang, D., Yang, Y., et al. (2019). The formation of nitro-aromatic compounds under high NO<sub>x</sub> and anthropogenic VOC conditions in urban Beijing, China. *Atmospheric Chemistry and Physics*, 19(11), 7649–7665. <https://doi.org/10.5194/acp-19-7649-2019>
- Xie, M. J., Chen, X., Hays, M. D., & Holder, A. L. (2019). Composition and light absorption of N-containing aromatic compounds in organic aerosols from laboratory biomass burning. *Atmospheric Chemistry and Physics*, 19(5), 2899–2915. <https://doi.org/10.5194/acp-19-2899-2019>
- Xie, M. J., Chen, X., Hays, M. D., Lewandowski, M., Offenberg, J., Kleindienst, T. E., & Holder, A. L. (2017). Light absorption of secondary organic aerosol: Composition and contribution of nitroaromatic compounds. *Environmental Science & Technology*, 51(20), 11607–11616. <https://doi.org/10.1021/acs.est.7b03263>
- Xu, C., & Wang, L. (2013). Atmospheric oxidation mechanism of phenol initiated by OH radical. *Journal of Physical Chemistry A*, 117(11), 2358–2364. <https://doi.org/10.1021/jp308856b>
- Yan, F., Chen, W., Jia, S., Zhong, B., Yang, L., Mao, J., et al. (2020). Stabilization for the secondary species contribution to PM<sub>2.5</sub> in the Pearl River Delta (PRD) over the past decade, China: A meta-analysis. *Atmospheric Environment*, 242, 117817. <https://doi.org/10.1016/j.atmosenv.2020.117817>
- Yang, B., Zhang, H., Wang, Y., Zhang, P., Shu, J., Sun, W., & Ma, P. (2016). Experimental and theoretical studies on gas-phase reactions of NO<sub>3</sub> radicals with three methoxyphenols: Guaiacol, creosol, and syringol. *Atmospheric Environment*, 125, 243–251. <https://doi.org/10.1016/j.atmosenv.2015.11.028>
- Yassine, M. M., Harir, M., Dabek-Zlotorzynska, E., & Schmitt-Kopplin, P. (2014). Structural characterization of organic aerosol using Fourier transform ion cyclotron resonance mass spectrometry: Aromaticity equivalent approach. *Rapid Communications in Mass Spectrometry*, 28(22), 2445–2454. <https://doi.org/10.1002/rcm.7038>
- Yuan, B., Liggio, J., Wentzell, J., Li, S.-M., Stark, H., Roberts, J. M., et al. (2016). Secondary formation of nitrated phenols: Insights from observations during the Uintah Basin Winter Ozone Study (UBWOS) 2014. *Atmospheric Chemistry and Physics*, 16(4), 2139–2153. <https://doi.org/10.5194/acp-16-2139-2016>
- Zhang, Q., Sarkar, S., Wang, X., Zhang, J., Mao, J., Yang, L., et al. (2019). Evaluation of factors influencing secondary organic carbon (SOC) estimation by CO and EC tracer methods. *The Science of the Total Environment*, 686, 915–930. <https://doi.org/10.1016/j.scitotenv.2019.05.402>
- Zhang, X., Lin, Y. H., Surratt, J. D., & Weber, R. J. (2013). Sources, composition and absorption Angstrom exponent of light-absorbing organic components in aerosol extracts from the Los Angeles Basin. *Environmental Science & Technology*, 47(8), 3685–3693. <https://doi.org/10.1021/es305047b>

## References From the Supporting Information

- Engling, G., Carrico, C. M., Kredlenweis, S. M., Collett, J. L., Jr., Day, D. E., Malm, W. C., et al. (2006). Determination of levoglucosan in biomass combustion aerosol by high-performance anion-exchange chromatography with pulsed amperometric detection. *Atmospheric Environment*, 40, S299–S311. <https://doi.org/10.1016/j.atmosenv.2005.12.069>
- Hennigan, C. J., Izumi, J., Sullivan, A. P., Weber, R. J., & Nenes, A. (2015). A critical evaluation of proxy methods used to estimate the acidity of atmospheric particles. *Atmospheric Chemistry and Physics*, 15(5), 2775–2790. <https://doi.org/10.5194/acp-15-2775-2015>
- Iinuma, Y., Engling, G., Puxbaum, H., & Herrmann, H. (2009). A highly resolved anion-exchange chromatographic method for determination of saccharidic tracers for biomass combustion and primary bio-particles in atmospheric aerosol. *Atmospheric Environment*, 43(6), 1367–1371. <https://doi.org/10.1016/j.atmosenv.2008.11.020>
- Kendrick, E. (1962). A mass scale based on CH<sub>2</sub> = 14.000 for high resolution mass spectrometry of organic compounds. *Analytical Chemistry*, 35(13), 2146–2154. <https://doi.org/10.1021/ac60206a048>
- Kitanovski, Z., Hovorka, J., Kuta, J., Leoni, C., Prokes, R., Sanka, O., et al. (2020). Nitrated monoaromatic hydrocarbons (nitrophenols, nitrocatechols, nitrosalicylic acids) in ambient air: Levels, mass size distributions and inhalation bioaccessibility. *Environmental Science and Pollution Research*, 28(42), 59131–59140.
- Koch, B. P., Dittmar, T., Witt, M., & Kattner, G. (2007). Fundamentals of molecular formula assignment to ultrahigh resolution mass data of natural organic matter. *Analytical Chemistry*, 79(4), 1758–1763. <https://doi.org/10.1021/ac061949s>
- Lin, P., Yu, J. Z., Engling, G., & Kalberer, M. (2012). Organosulfates in humic-like substance fraction isolated from aerosols at seven locations in East Asia: A study by ultra-high-resolution mass spectrometry. *Environmental Science & Technology*, 46(24), 13118–13127. <https://doi.org/10.1021/es303570v>
- Ma, Y. Q., Cheng, Y. B., Qiu, X. H., Cao, G., Fang, Y. H., Wang, J. X., et al. (2018). Sources and oxidative potential of water-soluble humic-like substances (HULISWS) in fine particulate matter (PM<sub>2.5</sub>) in Beijing. *Atmospheric Chemistry and Physics*, 18(8), 5607–5617. <https://doi.org/10.5194/acp-18-5607-2018>
- Nannoolal, Y., Rarey, J., Ramjugernath, D., & Cordes, W. (2004). Estimation of pure component properties: Part 1. Estimation of the normal boiling point of non-electrolyte organic compounds via group contributions and group interactions. *Fluid Phase Equilibria*, 226, 45–63. <https://doi.org/10.1016/j.fluid.2004.09.001>
- Pluskal, T., Castillo, S., Villar-Briones, A., & Oresic, M. (2010). MZmine 2: Modular framework for processing, visualizing, and analyzing mass spectrometry-based molecular profile data. *BMC Bioinformatics*, 11(1), 395. <https://doi.org/10.1186/1471-2105-11-395>
- Song, S., Gao, M., Xu, W., Shao, J., Shi, G., Wang, S., et al. (2018). Fine-particle pH for Beijing winter haze as inferred from different thermodynamic equilibrium models. *Atmospheric Chemistry and Physics*, 18(10), 7423–7438. <https://doi.org/10.5194/acp-18-7423-2018>
- Tong, H., Kourtchev, I., Pant, P., Keyte, I. J., O'Connor, I. P., Wenger, J. C., et al. (2016). Molecular composition of organic aerosols at urban background and road tunnel sites using ultra-high-resolution mass spectrometry. *Faraday Discussions*, 189, 51–68. <https://doi.org/10.1039/c5fd00206k>

- Turpin, B. J., & Lim, H. J. (2001). Species contributions to  $PM_{2.5}$  mass concentrations: Revisiting common assumptions for estimating organic mass. *Aerosol Science and Technology*, 35(1), r602–610. <https://doi.org/10.1080/02786820119445>
- Wang, L., Wang, X., Gu, R., Wang, H., Yao, L., Wen, L., et al. (2018). Observations of fine particulate nitrated phenols in four sites in northern China: Concentrations, source apportionment, and secondary formation. *Atmospheric Chemistry and Physics*, 18(6), 4349–4359. <https://doi.org/10.5194/acp-18-4349-2018>
- Wang, Y., Hu, M., Wang, Y.-C., Li, X., Fang, X., Tang, R., et al. (2020). Comparative study of particulate organosulfates in contrasting atmospheric environments: Field evidence for the significant influence of anthropogenic sulfate and  $NO_x$ . *Environmental Science and Technology Letters*, 7(11), 787–794. <https://doi.org/10.1021/acs.estlett.0c00550>
- Weber, R. J., Guo, H., Russell, A. G., & Nenes, A. (2016). High aerosol acidity despite declining atmospheric sulfate concentrations over the past 15 years. *Nature Geoscience*, 9(4), 282–285. <https://doi.org/10.1038/ngeo2665>
- Xing, L., Fu, T. M., Cao, J. J., Lee, S. C., Wang, G. H., Ho, K. F., et al. (2013). Seasonal and spatial variability of the OM/OC mass ratios and high regional correlation between oxalic acid and zinc in Chinese urban organic aerosols. *Atmospheric Chemistry and Physics*, 13(8), 4307–4318. <https://doi.org/10.5194/acp-13-4307-2013>
- Zhang, Y. Y., Mueller, L., Winterhalter, R., Moortgat, G. K., Hoffmann, T., & Poeschl, U. (2010). Seasonal cycle and temperature dependence of pinene oxidation products, dicarboxylic acids and nitrophenols in fine and coarse air particulate matter. *Atmospheric Chemistry and Physics*, 10(16), 7859–7873. <https://doi.org/10.5194/acp-10-7859-2010>